SAVE PRINT

NOTICE: Use the buttons above to print the form (Reader and Exchange) or to save the form (Exchange). DO NOT use the Netscape tool bar.

LA-UR- 05-5735

Approved for public release; distribution is unlimited.

Title: Effective Propagation Kernels in Structured Media with Broad Spatial Correlations, Illustration with Large-scale Transport of Solar Photons Through Cloudy Atmospheres

Author(s): Anthony B. Davis,
Space & Remote Sensing Sciences Group (ISR-2)

Submitted to: Computational Methods in Transport - Granlibakken 2004
(Lecture Notes in Computational Science and Engineering, vol. 48),
F. Graziani (Ed.),
Springer, New York (NY),
pp. 85-140 (2006)

SAVE PRINT CLEAR FORM

Los Alamos
NATIONAL LABORATORY

Effective Propagation Kernels in Structured Media with Broad Spatial Correlations, Illustration with Large-Scale Transport of Solar Photons Through Cloudy Atmospheres

Anthony B. Davis

Los Alamos National Laboratory, Space & Remote Sensing Sciences Group
ISR-2, P.O. Box 1663, Los Alamos, New Mexico, USA, adavis@lanl.gov

Summary. It is argued that, to directly target the mean fluxes through a structured medium with spatial correlations over a significant range of scales that includes the mean-free-path, one can use an effective propagation kernel that will necessarily be sub-exponential. We come to this conclusion using both standard transport theory for variable media and a point-process approach developed recently by A. Kostinski. The ramifications of this finding for multiple scattering and effective medium theory are examined. Finally, we describe a novel one-dimensional transport theory with asymptotically power-law propagation kernels and use it to shed new light onto recent observations of solar photon pathlength in the Earth's cloudy atmosphere.

1 Introduction and Overview

We start with a compact (operator-based) formulation of the monokinetic linear transport problem in higher-dimensions of sufficient generality for our present needs. Phase-space density (times velocity c), denoted $I(\boldsymbol{x},\boldsymbol{\Omega})$, is called "specific intensity" or "radiance" in the parlance of radiative transfer (RT) theory. It is determined by a one-group linear Boltzman equation [1]

$$\mathcal{L}I = \mathcal{S}I + Q \tag{1}$$

where

$$\mathcal{L} = \boldsymbol{\Omega} \bullet \nabla + \sigma(\boldsymbol{x}) \tag{2}$$

describes the advection and extinction of particle beams while

$$\mathcal{S} = \sigma_{\rm s}(\boldsymbol{x}) \int\limits_{4\pi} p(\boldsymbol{x},\boldsymbol{\Omega}' \to \boldsymbol{\Omega})[\cdot]{\rm d}\boldsymbol{\Omega}' \tag{3}$$

describes the volume scattering process, and $Q(\boldsymbol{x},\boldsymbol{\Omega})$ is the volume source term. We will call this the "3D RT equation" (here, in its integro-differential incarnation). We also need boundary conditions (BCs) which can often be taken as vacuum (no incoming radiance) or reflective (which is just like scattering but at a surface).

Most numerical solutions of this problem use, in one way or another, the equivalent integral equation

$$I = \mathcal{K}I + I_0 \tag{4}$$

that naturally incorporates the BCs; here

$$\mathcal{K} = \mathcal{L}^{-1}\mathcal{S} \tag{5}$$

is the *transport* kernel while

$$I_0 = \mathcal{L}^{-1}Q \tag{6}$$

represents the uncollided particles. The integral operator $\mathcal{L}^{-1}$ is the main focus of this paper; we will call it the *propagation* kernel. Formally, one can write the solution of (4) as

$$I = \frac{I_0}{1-\mathcal{K}} = \sum_{n=0}^{\infty} \mathcal{K}^n I_0, \tag{7}$$

the well-known Neumann series.

In this paper however, we are not interested in a solutions of fully specified (deterministic) 3D RT problems. Rather, we are interested in the mean and other statistical properties of solutions averaged over many realizations of the spatial variability: "mean-field" RT theory where the parameters of interest are also means, variances, covariances, correlation functions, and so on, evaluated for the optical properties of the media. Typically, assumptions are made in such a way that these *ensemble* averages at a point will be invariant under a relevant class of translations and rotations: statistical homogeneity and isotropy prevails. These point transformations need not be fully 3D; for instance, they can be only in the horizontal plane. So what we call here a mean-field RT solution is often thought of as a model for large-scale averages in the statistically invariant spatial dimensions.

The most venerable approach to this challenging problem was pioneered[1] by the regretted transport theoretician extraordinaire G. C. Pomraning (1936–1999) along with his students and coworkers. The interested reader is referred to his definitive text *Linear Kinetic Theory and Particle Transport in Stochastic Mixtures* [3]. In this framework, tractable problems with scattering are limited to Markovian binary media: two types of material and uniform probabilities of crossing a boundary per unit of length along any beam. There are only two structural parameters: the volume mixing ratio and the characteristic scale of the clumps of the less abundant material. One ends up here with the likes of two integro-differential equations for uniform media to solve simultaneously because they are coupled by linear exchange terms.

Other statistical RT models, inspired by the phenomenology of turbulence, have been based on scale-wise expansions (as in Fourier space) and closure methods, e.g., Stephens [4]. Yet other methods simply prescribe averaging over solutions of homogeneous problems using 1-point statistics and thus foregoing any impact of spatial correlations, e.g., Barker [5]. For further examples in atmospheric science, primarily motivated by large-scale radiation budget considerations in climate studies, see the recent survey by Barker and Davis [6].

A very desirable outcome of a statistical RT model from any of the above approaches is "homogenization:" compute effective optical medium properties that can

[1] This is on the US side of the Cold War. In the former USSR, parallel developments happened starting, as far as I know, with Avaste and Vainikko's [2] investigation of broken clouds and continue to this day.

be applied to a homogeneous RT problem, but that somehow to capture the effects of the unresolved variability. For instance, Graziani and Slone [7] seek an effective mean free path dependent on structural parameters of Markovian and other media in order to treat them with a single RT equation. An example in cloud radiation is Cahalan's [8] rescaled optical depth model which is based on straightforward 1-point/single-variable averaging of solutions of the standard 1D RT problem when cloud optical depth is positively skewed (e.g., lognormal-like). Another notable example in atmospheric science is Cairns et al.'s [9] renormalization of all local optical properties which is grounded in a sophisticated Green function analysis.[2] of the 3D RT problem and also adapts powerful techniques from contemporary statistical physics.

A common trait of the above methods that care at all about covariances [4] or spatial correlations [10, 9, 11] is the (often implicit) requirement that the variability scales and the averaging scales be well-separated. In cloudy atmospheres however, and probably also in many other structured media dominated by turbulent reactive flows, spatial correlations are "long-range" (typically power-law wavenumber spectra are observed). It is therefore not obvious that we can observe scales where the statistics can be deemed homogeneous and that one can really talk about variability confined to a certain range of scales.

Although Cairns et al. [9] correctly averages the iterated *transport* kernel $\mathcal{K}^n$ in (7) with the spatial ($\mathcal{L}^{-1}$) and angular ($\mathcal{S}$) aspects inherently intertwined in $(\mathcal{L}^{-1}\mathcal{S})^n$, the remainder of this paper is essentially an attempt at treating them separately and relating this approximation to the general idea of diffusion. There is little theoretical justification for this separation beyond connection with Lévy walks, a popular model in both statistical physics [12] and in stochastic processes [13]. Nonetheless, recent observations of multiply scattered sunlight in the Earth's cloudy atmosphere [14, 15] support this approximation that we revisit further on.

In the following Section, we revisit the basic physics of extinction (i.e., σ) and scattering (i.e., $\sigma_s p(\mathbf{\Omega}' \to \mathbf{\Omega})$), introducing some useful notation in the process. We then examine in Sect. 3 the general properties of averaged free-path distributions in random but spatially-correlated 3D media as determined by $\langle \mathcal{L}^{-1} \rangle$ where the angular brackets denote ensemble/spatial averages; we do this from two different standpoints, RT theory and point processes. This enables us to state a fundamental limitation of effective medium theory that may or may not impact practical implementations. We also look at the form of $\langle \mathcal{L}^{-1} \rangle$ for the specific kind of variability observed in the Earth's cloudy atmosphere. In Sect. 4, we return to multiple scattering transport by first showing, under quite general conditions, that angular diffusion makes iterates of $\mathcal{S}$ very close to projections onto the space of isotropic functions $U(\boldsymbol{x})$ —physically, photon density— in finite time; it is then relatively easy to obtain the asymptotic behavior of $\mathcal{K}^n \approx \langle \mathcal{L}^{-1} \rangle^n$ for both infinite and finite media, assuming complete angular redistribution. In Sect. 5, we display some recently published absorption-based diagnostics of solar photon transport through real 3D clouds and propose a simple 1D RT model based on the relevant family of propagation kernels $\langle \mathcal{L}^{-1} \rangle$ that explains these observations. We offer some concluding remarks in Sect. 6.

I have already started and will continue to use the language of radiative transfer (photons, extinction, optics, etc.), and furthermore in the frame of atmospheric

[2] Uses the solutions G of (1) when Q is a roaming Dirac δ source; formally, we have $G = (\mathcal{L} - \mathcal{S})^{-1}$.

science. Much of the following is nonetheless applicable to neutron or neutrino transport in engineering or astrophysical systems.

2 Extinction and Scattering Revisited, and Some Notations Introduced

2.1 The Extinction Coefficient

The simplest description of matter-radiation interaction is photon depletion when a narrow collimated beam crosses an optical medium, cf. left-hand side of Fig. 1 where it is assumed that $\delta I \geq 0$. We have basically expressed here the flux-divergence theorem for an "elementary" kinetic volume of length $\delta\ell$. Along the horizontal cylinder the net transport is 0; to the left, there is an in-flux I; to the right, an out-flux $I-\delta I$. So the divergence integral is simply the difference from left to right. Operationally, we have

$$\delta I \propto I \times \delta\ell \tag{8}$$

and the proportionality constant, defined as

$$\sigma = \lim_{\delta\ell\to 0} \frac{\delta I/I}{\delta\ell} \ ... \text{ in } \mathrm{m}^{-1}, \tag{9}$$

is the *extinction coefficient* or simply "extinction."

What is the detailed mechanism of extinction? This is about a population of streaming photons colliding with an essentially static population of massive particles. So all we have to do is estimate the number of particles in the sample volume in Fig. 1: $\delta N = n\delta A\delta\ell$. Multiplying this by the (mean) cross-section $\mathtt{s}$ and dividing by δA yields the element of probability for an interaction which, by definition (9), is $\sigma\delta\ell$, and should be $\ll$1. Thus, as some position $(\boldsymbol{x})$, we have

$$\sigma(\boldsymbol{x}) = n(\boldsymbol{x}) \times \mathtt{s}. \tag{10}$$

In this sense, extinction is the interaction cross-section per unit of volume, equivalently, the probability of collision per unit of length. Note that the medium as to be sufficiently dilute ($n^{-1/3} \gg \mathtt{s}^{1/2}$); otherwise (tightly-packed particles), it is wrong to think that a small distance $\delta\ell$ in $\mathtt{s}n \times \delta\ell$ makes it a small element of probability.

In (10), the cross-section $\mathtt{s}$ is for *any* kind of interaction by *any* kind of particle. In radiative transfer, it is naturally partitioned between absorption (photon destruction) and scattering (photon re-direction).[3] This partition carries over immediately to the transport coefficients:

$$\sigma(\boldsymbol{x}) = \sigma_\mathrm{a}(\boldsymbol{x}) + \sigma_\mathrm{s}(\boldsymbol{x}). \tag{11}$$

[3] In neutronics, there is a third elementary process: multiplication, which is basically an "anti-absorption;" formally, we model this process with $\sigma_\mathrm{a} < 0$ (an isotropic source of particles that is $\propto I$). In optics, there is stimulated emission which can dominate in NTLE situations, such as in laser cavities. Because of the tight correlation between the incoming and outgoing photon's directions, this is best modeled as a negative extinction in (9).

In environmental and astrophysical applications, there is often a mixture of optically relevant material particles in the kinetic volume in terms of size (cf. right-hand side of Fig. 1), shape, chemistry, etc. An important quantity in the following is single-scattering albedo:

$$\varpi_0(\boldsymbol{x}) = \sigma_\mathrm{s}(\boldsymbol{x})/\sigma(\boldsymbol{x}). \tag{12}$$

We can then express the absorption coefficient as

$$\sigma_\mathrm{a}(\boldsymbol{x}) = [1 - \varpi_0(\boldsymbol{x})]\,\sigma(\boldsymbol{x}), \tag{13}$$

where $1 - \varpi_0(\boldsymbol{x})$ is sometimes called the "co-albedo" for single scattering.

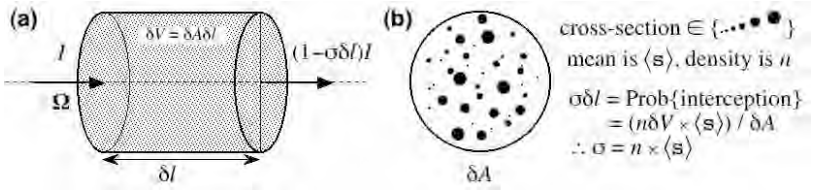

Fig. 1. Mechanism of optical extinction by a dilute medium of scattering/absorbing particles: **(a)** elementary cylindrical volume, **(b)** photon beam's view down the axis of the cylinder when a variety of cloud droplet sizes are present. Adapted from Fig. 3.7 in [16]

As long as the overarching condition of weak dilution is verified, we can use the linearity of (10)–(11) to simply sum the cross-sections $\mathbf{s}^{(\mathrm{s})}$ and $\mathbf{s}^{(\mathrm{a})}$ (for scattering and absorption respectively) of different types of photon-intercepting particles weighted by the associated densities:

$$\sigma_{\mathrm{a,s}}(\boldsymbol{x}) = \sum_{\text{species } i} \mathbf{s}_i^{(\mathrm{a,s})} \times n_i(\boldsymbol{x}). \tag{14}$$

A variation of this principle is when the "species" are defined by a continuously varying parameter such as size r:

$$\sigma_{\mathrm{a,s}}(\boldsymbol{x}) = \int_0^\infty \mathbf{s}^{(\mathrm{a,s})}(r) \times \frac{\mathrm{d}n}{\mathrm{d}r}(r;\boldsymbol{x})\,\mathrm{d}r. \tag{15}$$

For spherical particles (such as cloud droplets) of radius r, Mie scattering theory specifies the efficiency factor $Q_{(\mathrm{a,s})}(2\pi r/\lambda)$ that appears in $\mathbf{s}^{(\mathrm{a,s})}(r) = \pi r^2 \times Q_{(\mathrm{a,s})}(2\pi r/\lambda)$ where λ is the given wavelength, cf. Deirmendjian [17] for standard size spectra $\mathrm{d}n/\mathrm{d}r$ used in atmospheric optics.

Interesting questions arise when a particle type or size can not be considered uniformly distributed at any scale, i.e., that it is impossible to define a density $n_i(\boldsymbol{x})$ or $\mathrm{d}n/\mathrm{d}r(r;\boldsymbol{x})$. I refer to Knyazikhin et al. [18] for an investigation of more general formulations of the extinction problem that capture this case. In the next section, we will proceed to investigate spatial variability effects under the weak assumption that at least the dominant types of particles have well-defined local densities.

2.2 The Scattering Phase Function

Figure 2 illustrates the redistribution of radiant energy between different beams through scattering. Our goal is to estimate the element of scattered flux δF_s. It is surely proportional to the small solid angle into which the scattering occurs $\delta\mathbf{\Omega}$ and to the small loss of flux δF_0 incurred when the incoming photons cross the sample volume (conditional to scattering rather than absorption); the latter term is equal to the scattering coefficient times the small length $\delta\ell$. In summary, we have

$$\delta F_\mathrm{s} \propto \delta F_0 \delta\mathbf{\Omega} = F_0 \sigma_\mathrm{s} \delta\ell \times \delta\mathbf{\Omega}. \tag{16}$$

We define the scattering phase function as

$$p(\mathbf{\Omega}_0 \to \mathbf{\Omega}) = \lim_{\delta\ell, \delta\mathbf{\Omega} \to 0} \frac{\delta F_\mathrm{s}}{\delta F_0 \times \delta\mathbf{\Omega}} \ \ldots \text{ in } \mathrm{sr}^{-1} \tag{17}$$

which will generally depend on position $\boldsymbol{x}$ as well as one or two angular variables: the scattering angle $\theta_\mathrm{s} = \cos^{-1}(\mathbf{\Omega}_0 \bullet \mathbf{\Omega})$ and, possibly, an azimuthal scattering angle as well. As an example that we will return to latter on, consider everywhere isotropic scattering:

$$p(\boldsymbol{x}, \mathbf{\Omega}_0 \to \mathbf{\Omega}) \equiv 1/4\pi. \tag{18}$$

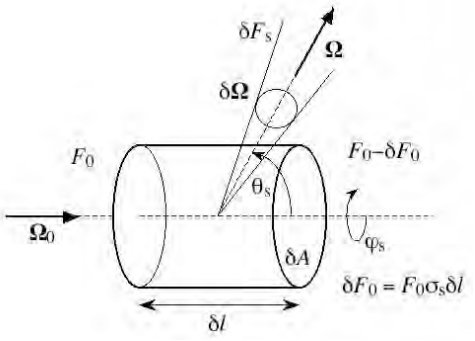

Fig. 2. Schematic of scattered radiance. Adapted from Fig. 3.8 in [16]

As for extinction, let us have a closer look at the mechanics of scattering at the individual collision level.[4] To isolate the inherent property of the scattering medium, we compute

[4] In the context of RT, it is technically incorrect to think of a photon as being scattered since its identity, as an eigen-mode of the quantized EM equations, is defined in particular by its direction of propagation. However, a quantum hc/λ of radiant energy is transfered between modes at each elastic scattering, and I will continue the tradition of calling this the scattering of "a photon." In RT per se, "photon" is in fact short for photon beam since we are in the classic limit of geometric optics where all distances of interest are much larger than the

$$\lim_{\delta s,\delta\boldsymbol{\Omega}\to 0}\frac{\delta F_{\mathrm{s}}/F_0}{\delta s\times\delta\boldsymbol{\Omega}}=\sigma_{\mathrm{s}}(\boldsymbol{x})p(\boldsymbol{x},\boldsymbol{\Omega}_0\to\boldsymbol{\Omega})=n(\boldsymbol{x})\times\frac{\mathrm{d}\mathbf{s}}{\mathrm{d}\boldsymbol{\Omega}}(\boldsymbol{x},\boldsymbol{\Omega}_0\to\boldsymbol{\Omega}) \tag{19}$$

where the last expression is obtained by straightforward generalization of (10) to *differential* cross-sections. As for extinction in (15), differential cross-section should be averaged over the population of particles in the sample volume in terms of size and/or type.

By radiant energy conservation, we have

$$\int_{4\pi}p(\boldsymbol{x},\boldsymbol{\Omega}_0\to\boldsymbol{\Omega})\mathrm{d}\boldsymbol{\Omega}\equiv 1,\ \forall\boldsymbol{x},\boldsymbol{\Omega}. \tag{20}$$

By optical reciprocity, we have $p(\boldsymbol{x},\boldsymbol{\Omega}\to\boldsymbol{\Omega}_0)=p(\boldsymbol{x},\boldsymbol{\Omega}_0\to\boldsymbol{\Omega})$, hence

$$\int_{4\pi}p(\boldsymbol{x},\boldsymbol{\Omega}_0\to\boldsymbol{\Omega})d\boldsymbol{\Omega}_0\equiv 1,\ \forall\boldsymbol{x},\boldsymbol{\Omega}_0. \tag{21}$$

In the remainder of this section, I will assume the spatial variability the phase function is implicit, and drop $\boldsymbol{x}$ from its arguments.

In most atmospheric applications (high-altitude cirrus clouds made of ice-crystals being the notable exception), it is reasonable to assume that scattering is axi-symmetric around the incoming beam. Hence,

$$p(\boldsymbol{\Omega}_0\to\boldsymbol{\Omega})\equiv p(\boldsymbol{\Omega}_0\bullet\boldsymbol{\Omega})=p(\mu_{\mathrm{s}}). \tag{22}$$

where the scattering angle θ_{s} is given by $\mu_{\mathrm{s}}=\cos\theta_{\mathrm{s}}=\boldsymbol{\Omega}_0\bullet\boldsymbol{\Omega}$.

This enables an expansion of the phase function in spherical harmonics (eigenfunctions of $\mathcal{S}$) without the complication of azimuthal terms:

$$p(\mu_{\mathrm{s}})=\frac{1}{4\pi}\sum_{n\geq 0}(2n+1)\eta_n P_n(\mu_{\mathrm{s}}), \tag{23}$$

where $P_n(x)$ is th nth-order Legendre polynomial. These coefficients are computed from

$$\eta_n=2\pi\int_{-1}^{+1}P_n(\mu_{\mathrm{s}})p(\mu_{\mathrm{s}})\mathrm{d}\mu_{\mathrm{s}}. \tag{24}$$

Specific values of the Legendre polynomials can be obtained efficiently by recursion but their analytical expressions are best derived from the generating function [19]

$$\Phi(x,z)=\sum_{n\geq 0}P_n(x)z^n=\frac{1}{\sqrt{1-2xz+z^2}}, \tag{25}$$

for $|x|$ and $|z|<1$. Using

wavelength λ. Physical (wave-theoretical) optics are required only to compute transport coefficients at the individual cross-section level, which can indeed be on the order of the wavelength squared. The weak dilution requirement and the usual assumption of *uncorrelated* random positions then ensures that we can add intensities (energies) rather than amplitudes and phases to model the behavior of photon beams.

$$P_n(x) = \frac{1}{n!}\left(\frac{\partial}{\partial z}\right)^n \Phi(x,z)\bigg|_{z=0}, \tag{26}$$

we find $P_0(x) = 1, P_1(x) = x, P_2(x) = (3x^2-1)/2$, and so on. The orthogonality of the Legendre polynomials,

$$\int_{-1}^{+1} P_n(x)P_{n'}(x)\mathrm{d}x = \frac{\delta_{nn'}}{n+1/2}, \tag{27}$$

where $\delta_{nn'}$ is the Kronecker symbol, ensures diagonalization of the scattering operator $\mathcal{S}$ in spherical-harmonic space. It is therefore little surprise that virtually all grid-based (non-Monte Carlo) numerical solutions of the 3D RT equation exploit spherical harmonics.

We have $\eta_0 = 1$ by conservation for any phase function, and the only non-vanishing coefficient for isotropic scattering in (18). Also of considerable interest is

$$g = \eta_1 = 2\pi \int_{-1}^{+1} \mu_\mathrm{s} p(\mu_\mathrm{s})\mathrm{d}\mu_\mathrm{s}, \tag{28}$$

called the "asymmetry factor" or simply the mean cosine of the scattering angle. This last description of g correctly presents the phase function as a probability density function (PDF) in direction space, and this is indeed how $p(\mu_\mathrm{s})$ is used in Monte Carlo schemes. Any deviation of the phase function from isotropy corresponds to a directional correlation (in principle, of either sign) between incident and scattered photons.

I will be introducing several kinds of averages in upcoming section. So those that concern photon scattering and propagation events deserve a special notation, which I borrow from the probability literature: $\mathcal{E}(\cdot)$ which stands for (mathematical) *expectation* of the random variable in the argument. Thus, we can recast the asymmetry factor in (28) as

$$g = \mathcal{E}(\boldsymbol{\Omega}\bullet\boldsymbol{\Omega}_0) = \int_{4\pi} \boldsymbol{\Omega}\bullet\boldsymbol{\Omega}_0 \mathrm{d}P(\boldsymbol{\Omega}|\boldsymbol{\Omega}_0) \tag{29}$$

where $\mathrm{d}P(\boldsymbol{\Omega}|\boldsymbol{\Omega}_0) = p(\boldsymbol{\Omega}_0\bullet\boldsymbol{\Omega})\mathrm{d}\boldsymbol{\Omega}$. The "|" delimiter in a PDF separates the random variable from the given (fixed) quantities that need to be highlighted.

2.3 Henyey–Greenstein Models for the Phase Function

A very popular 1-parameter model for the single-scattering process in atmospheric optics and elsewhere is the Henyey–Greenstein [20] phase function

$$p(\mu_\mathrm{s}; g) = \left(\frac{1}{4\pi}\right)\frac{1-g^2}{(1+g^2-2g\mu_\mathrm{s})^{3/2}}. \tag{30}$$

I will use the delimiter ";" to separate, as needed, variables from parameters in argument lists. I will also use subscripts, e.g., $p_g(\mu_\mathrm{s})$ in this case.

In spherical harmonics, the Henyey–Greenstein model (30) yields

$$\eta_n(g) = g^n. \tag{31}$$

Indeed, $4\pi p(x;z)$ is identical to $\sum_{n=0}^{\infty}(2n+1)P_n(x)z^n = 2\partial\Phi(x,z)/\partial z + \Phi(x,z)$ from (25); the above coefficients then follow by comparison with (23). This Legendre decomposition is used in virtually all numerical implementations of the scattering operator $\mathcal{S}$, except Monte Carlo (random quadrature) schemes where the simulation of the Markov chain requires the generation of random values of μ_s with the probability measure implicit in (30). In the case of the Henyey–Greenstein phase function, one can use the method of inverting the cumulative probability because the running integral of (30) with respect to μ_s has a simple expression. Specifically, one can generate random values of μ_s with

$$\mu_\mathrm{s} = \frac{1}{2g}\left(1 + g^2 - \left[\frac{1-g^2}{1+g(1-2\xi)}\right]\right),\ |g| \le 1,\ g \neq 0, \tag{32}$$

where ξ is a (pseudo-)random deviate uniformly distributed on the interval (0,1). When $g \to 0$, L'Hôpital's rule in (32) yields the expected result for isotropic scattering: $\mu_\mathrm{s} = 1 - 2\xi$. The azimuthal scattering angle is selected randomly: $\phi_\mathrm{s} = 2\pi\xi$.

Sometimes, it is useful to compute RT in reduced dimensionality. For instance, "3D" RT effects have been successfully investigated in 2D: one direction for the mean flux (z) and one other, at right angles, for the spatial variability (x). It is not necessary in this case to propagate photons in the 3rd dimension and the general representation for radiance is $I(x,z,\theta)$, where θ is still measured away from the z-axis. The small price to pay for this conceptual simplification is that all the geometrical units used so far must be adjusted:

- fluxes are now in $\mathrm{s}^{-1}\mathrm{m}^{-1}$;
- radiances are fluxes/rad since solid angles and direction (θ,ϕ) are now reduced to regular angles and just θ;
- extinction, scattering and absorption coefficients are still in m^{-1} but, if needed, "cross-sections" are in meters while densities are in m^{-2}; and finally,
- phase functions are in rad^{-1}.

To support studies in this kind of RT in "Flatland," Davis et al. [21] proposed a 2D version of the Henyey–Greenstein phase function:

$$p(\mu_\mathrm{s};g) = \lim_{\delta\tau_\mathrm{s},\delta\theta\to 0}\frac{\delta F_\mathrm{s}/F_0}{\delta\tau_\mathrm{s}\times\delta\theta} = \left(\frac{1}{2\pi}\right)\frac{1-g^2}{1+g^2-2g\mu_\mathrm{s}} \tag{33}$$

where τ_s is the element of (scattering) optical distance across the small 2D "volume" where the scattering occurs (think of a 2D version of Fig. 2). Note that the polar diagram of this 2D phase function, as a function of $\theta_\mathrm{s} = \cos^{-1}\mu_\mathrm{s}$, is an ellipse of eccentricity $2g/(1+g^2)$ with the scattering particle at a focus. The asymmetry factor g retains the same meaning in 2D it was given in 3D through (29): mean cosine of the scattering angle.

The 2D analog of the spherical harmonic decomposition (23)–(24) on the 3D unit sphere Ξ is a cosine Fourier series analysis on the interval $(-\pi,+\pi]$ where θ_s takes its values. Specifically,

$$p(\mu_\mathrm{s}) = \frac{1}{\pi}\sum_{n\ge 0}\frac{\eta_n}{1+\delta_{0n}}\cos n\theta_\mathrm{s} \tag{34}$$

where

$$\eta_n = \int_{-\pi}^{+\pi} p(\theta_\mathrm{s}) \cos n\theta_\mathrm{s} \mathrm{d}\theta_\mathrm{s}. \tag{35}$$

For the 2D Henyey–Greenstein phase function in (33), it can be shown that the nth Fourier coefficient in (35) is $\eta_n(g) = g^n$, just as in (31) for the 3D case. While this is useful in a numerical implementation of $\mathcal{S}$ in 2D for a spatially-gridded representation of the 2D radiance, a 2D Monte Carlo scheme would use

$$\theta_\mathrm{s} = 2\tan^{-1}\left(\frac{1-g}{1+g}\tan\left[\frac{\pi}{2}(1-2\xi)\right]\right), \ |g| \leq 1, \tag{36}$$

in lieu of (32).

The ultimate dimensionality reduction in RT is when the light particles can travel only on one axis, say, up or down. Here, fluxes (and/or radiances) are simply in s^{-1}, the extinction coefficient (like density) is in m^{-1} while cross-sections and the phase-function are dimensionless. Indeed, scattering in 1D amounts to either no change of direction of travel ($\mu_\mathrm{s} = +1$) or reversed direction ($\mu_\mathrm{s} = -1$). In this case, the angular PDFs in (30) or (33) are reduced to a Bernoulli trial:

$$p(\mu_\mathrm{s}; g) = \lim_{\delta\tau_\mathrm{s}\to 0} \frac{\delta F_\mathrm{s}/F_0}{\delta\tau_\mathrm{s}} = \begin{cases} \mu_\mathrm{s} = +1, & \text{with probability } (1+g)/2 \\ \mu_\mathrm{s} = -1, & \text{with probability } (1-g)/2 \end{cases}. \tag{37}$$

In other words,

$$p(\pm 1; g) = (1 \pm g)/2. \tag{38}$$

This is in fact the most general phase function in 1D. As in higher dimensions, g is still the mean of μ_s, the cosine of the scattering angle, even though it can take only 2 values.

RT in 1D is of course not a framework for investigating 3D effects. 1D RT is however an analytically tractable benchmark, at least when ϖ_0 and g are constant in the 1D medium.[5] In this model, the two 1D "radiances" are readily identified with 3D hemispherical fluxes in the upper- and lower halves ($\Xi_\pm$) of Ξ. It dates back at least to Schuster's seminal 1905 paper [22]. 1D RT has undeniable tutorial value. Amazingly, it is still used in many global climate models in one or another of its evolved but mathematically equivalent forms [23].

3 Propagation

3.1 Direct Transmission in 3D Media as a Problem in Stochastic ODEs

There is an apparently elementary calculus problem posed in (9), namely,

[5] In 1D, 2D or 3D, the extremal values of g, $+1$ and -1 are only of academic interest. They indeed lead to Dirac δ-functions in the respective scattering-angle spaces: $(\mu_\mathrm{s}, \phi_\mathrm{s}) \in \Xi$, $\theta_\mathrm{s} \in (-\pi, +\pi]$, $\mu_\mathrm{s} \in \{-1, +1\}$. For $g = +1$ scattering per se is defeated and the RT problem collapses onto the pure extinction/absorption/emission problem, which is 1D (beam-by-beam). For $g = -1$, we obtain a somewhat pathological 1D (beam-by-beam) transport model where propagation direction is switched at every scattering event.

$$\mathrm{d}I/I = \mathrm{d}\ln I = -\sigma(\boldsymbol{x})\mathrm{d}s, \tag{39}$$

which is easily solved by a change of variables $\mathrm{d}\tau(s) = \sigma(\boldsymbol{x})\mathrm{d}s$. We thus define *optical* distance as the running integral of σ along the beam $\boldsymbol{\Omega}_0$ from some starting point $\boldsymbol{x}_0$:

$$\tau(\boldsymbol{x}_0 \to \boldsymbol{x} = \boldsymbol{x}_0 + \boldsymbol{\Omega}_0 s) = \tau(s; \boldsymbol{x}_0, \boldsymbol{\Omega}_0) = \int_0^s \sigma(\boldsymbol{x}_0 + \boldsymbol{\Omega}_0 s')\mathrm{d}s'. \tag{40}$$

To address the problem of *cumulative* extinction, we will consider $(\boldsymbol{x}_0, \boldsymbol{\Omega}_0)$ to be fixed parameters. The solution of the ordinary differential equation (ODE) in (39) is therefore

$$I(s; \boldsymbol{x}_0, \boldsymbol{\Omega}_0) = I(0; \boldsymbol{x}_0, \boldsymbol{\Omega}_0)\exp[-\tau(s; \boldsymbol{x}_0, \boldsymbol{\Omega}_0)]. \tag{41}$$

This is the well-known exponential law of direct transmission with respect to *optical* distance.

Consider a uniform medium where optical distance is simply

$$\tau(\boldsymbol{x}_0 \to \boldsymbol{x} = \boldsymbol{x}_0 + \boldsymbol{\Omega}_0 s) = \sigma s, \ \forall \boldsymbol{x}_0, \boldsymbol{\Omega}_0; \tag{42}$$

thus

$$I(s) = I_0 \exp(-\sigma s). \tag{43}$$

This is Beer's law of exponential transmission with respect to *physical* distance. It is obviously of more limited applicability than (41).

Looking back at (39) and thinking of $\sigma(s; \boldsymbol{x}_0, \boldsymbol{\Omega}_0) = \sigma(\boldsymbol{x}_0 + \boldsymbol{\Omega}_0 s)$ as a random variable, we see that this is a problem in stochastic ODEs with multiplicative noise. The relevant questions in stochastic ODE theory are about the statistical properties of the solutions, in this case of $\exp[-\tau(s; \boldsymbol{x}_0, \boldsymbol{\Omega}_0)]$. Given that we will be interested in situations where the "noise" $\sigma(s; \boldsymbol{x}_0, \boldsymbol{\Omega}_0)$ has non-trivial correlation properties, we can not draw on the classic treatments [24].

First however, we examine the transport theoretical significance of the direct transmission law as a means of predicting the specifics of particle beam propagation.

3.2 Photon Free-Path Distributions

I have presented scattering as a random choice of new direction of propagation for the photon. There is also an inherent randomness in photon propagation which deserves to be re-examined from a probabilistic perspective.

From (41), but dropping the "0" subscripts for simplicity, we can derive *direct* transmission

$$T_{\mathrm{dir}}(s; \boldsymbol{x}, \boldsymbol{\Omega}) = \exp[-\tau(s; \boldsymbol{x}, \boldsymbol{\Omega})] = \Pr\{\text{step} \geq s | \boldsymbol{x}, \boldsymbol{\Omega}\} \tag{44}$$

by taking the ratio $I_{\mathrm{out}}/I_{\mathrm{in}} = I(s; \cdots)/I(0; \cdots)$. This is the probability of a photon to *not* suffer any kind of collision in an experiment over the *fixed* distance s, starting at $\boldsymbol{x}$ in direction $\boldsymbol{\Omega}$. Now think of the photon's free path or "step" to its next collision. As expressed above, $T_{\mathrm{dir}}(s; \boldsymbol{x}, \boldsymbol{\Omega})$ is the probability that this random variable exceeds s. So, thinking now of s as the random step length, its PDF is defined by

$$p(s|\boldsymbol{x}, \boldsymbol{\Omega})\mathrm{d}s = \mathrm{d}P(s|\boldsymbol{x}, \boldsymbol{\Omega}) = \Pr\{s \leq \text{step} < s + \mathrm{d}s | \boldsymbol{x}, \boldsymbol{\Omega}\}. \tag{45}$$

In terms of the 3D variability of the optical medium, this leads to

$$p(s|\boldsymbol{x},\boldsymbol{\Omega}) = \left(\frac{\mathrm{d}}{\mathrm{d}s}\right) P(s|\boldsymbol{x},\boldsymbol{\Omega}) = \sigma(\boldsymbol{x}+\boldsymbol{\Omega}s)\exp[-\tau(s;\boldsymbol{x},\boldsymbol{\Omega})], \tag{46}$$

using (40) and (44).

Consider the case of *uniform* extinction σ, the only quantity required in the problem at hand. The resulting free-path distribution (FPD) is given by

$$p(s|\sigma) = \sigma \mathrm{e}^{-\sigma s} \tag{47}$$

follows directly from above, or using Beer's exponential law of direct transmission in (43).

The cumulative extinction (optical distance) computation in (40) and of direct transmission in (44) is executed repetitively in many numerical solutions of the RT equation, and the Monte Carlo technique is no exception. In uniform media, the method of inverse cumulative probability follows directly from (47): the random length $s > 0$ of the step between two successive scattering events is given by

$$s = -\ln \xi/\sigma. \tag{48}$$

In 3D media, one draws randomly an optical distance to cover $\tau = -\ln \xi > 0$ and then one solves iteratively the equation in (40) for s.

The power of the differential formulation in (39) is that the collision accounting is always done in the "safe" regime where interaction probability is small. Then, conditional to survival, the collision probability is again assessed, and so on. The resulting exponential free-path distribution therefore follows directly from the inherent "lack-of-memory" in the course of the beam propagation. This is called a *Markov property* in probability theory.

There is in fact another even more tutorial way of deriving the above FPDs (PDFs for s) by returning to the basic definition of extinction in (9) and exploiting the photon's lack of memory about its past: whether it collides or not with a particle in the next instant does not depend on how far it has been traveling. So we can mentally divide s into $M \gg 1$ small segments of equal length and consider the probability of a photon crossing all of them without colliding with a particle. Since the collision probabilities $\delta I/I \approx \sigma\delta s$ where $\delta s = 1/M$ are independent in each sub-segment, the cumulative survival probability is by definition

$$T_{\mathrm{dir}}(\sigma s) \approx (1-\sigma s/M)^M. \tag{49}$$

Taking the limit $M \to \infty$ leads back to (41), hence to the FPD in (47). This proof, used in textbooks such as [25], easily generalizes to the case where σ varies along the beam's path, leading back to (40)–(41) hence to the FPD in (46).

3.3 Mean-Free-Path and Other Moments

A fundamental quantity in transport theory, for light quanta or any other type of particle, is the mean free path (MFP) given by

$$\ell(\boldsymbol{x},\boldsymbol{\Omega}) = \mathcal{E}(s|\boldsymbol{x},\boldsymbol{\Omega}) = \int_0^\infty s\mathrm{d}P(s|\boldsymbol{x},\boldsymbol{\Omega}). \tag{50}$$

Other moments of the FPD are also of general interest:

$$\mathcal{E}(s^q|\boldsymbol{x},\boldsymbol{\Omega}) = \int_0^\infty s^q \mathrm{d}P(s|\boldsymbol{x},\boldsymbol{\Omega}). \tag{51}$$

Reconsider the uniform-σ case in (47). We find

$$\ell(\sigma) = \mathcal{E}(s) = 1/\sigma. \tag{52}$$

So the optical distance given in (42), $\tau = \sigma s$, is just physical distance s in units of MFPs. Free-path moments of arbitrary order $q > -1$ can be computed from the exponential distribution in (47) and we find

$$\mathcal{E}(s^q) = \Gamma(q+1)/\sigma^q = \Gamma(q+1)\ell(\sigma)^q \tag{53}$$

where $\Gamma(\cdot)$ is Euler's Gamma function:

$$\Gamma(x) = \int_0^\infty t^{x-1}\mathrm{e}^{-t}\mathrm{d}t. \tag{54}$$

Recall that, for integer-valued arguments, $\Gamma(n+1) = n!,\ n \in \mathbb{N}$. In particular, the root-mean-square (RMS) free-path is given by

$$\sqrt{\mathcal{E}(s^2)} = \sqrt{2}/\sigma = \sqrt{2}\,\mathcal{E}(s). \tag{55}$$

It is larger than the MFP in (52), as required by Schwartz's inequality.

Schwartz's well-known inequality is equivalent in probability theory to the statement that variance,

$$\mathcal{D}(s) = \mathcal{E}([s - \mathcal{E}(s)]^2) = \mathcal{E}(s^2) - \mathcal{E}(s)^2, \tag{56}$$

is non-negative. Jensen's inequality in probability theory is less known in general. It is usually stated as

$$\mathcal{E}[f(X)] \geq f[\mathcal{E}(X)] \tag{57}$$

for any random variable X on the support of f and for any *convex* function f (i.e., $f'' > 0$ if f is everywhere twice differentiable on the support of the PDF of X). The "=" in (57) is obtained only in two situations:

1. f is linear in X;
2. X is sure (its variance is zero).

Schwartz's inequality is a special case of Jensen's with $f(X) = X^2$ being a *convex* function on the real axis $\mathbb{R}$. Jensen's inequality, or its converse for *concave* functions, will be repeatedly invoked further on.

3.4 Enhanced, Non-Exponential Steps in Spatially Correlated Media

I'll demonstrate here that, in media with variable extinction, the MFP is always larger than in a uniform medium associated with the mean extinction, equivalently, with the same overall number of particles according to (10). I'll also show that the *effective* FPD is always wider-than-exponential, even if the actual MFP is used. Detailed proofs are provided by Kostinski [26] and Davis and Marshak [27], respectively from the standpoints of non-Poissonian point processes and variable extinction fields. The importance of spatial correlations in the extinction field $\sigma(\boldsymbol{x})$ is emphasized in both studies, and echoed here.

Non-Uniform Extinction Field Approach

Let $\mathrm{M} \subseteq \mathbb{R}^3$ denote the 3D optical medium of interest. Using shorthand from probability theory, we define

$$\Pr(\mathrm{d}\sigma) = \Pr\{\boldsymbol{x} \in \mathrm{M} : \ \sigma \leq \ \text{extinction at } \boldsymbol{x} < \sigma + \mathrm{d}\sigma\} \tag{58}$$

for the 1-point variability of the extinction coefficient. Technically, the bracketed entity is a sub-set of M. In the random field theory used here, we will not need to distinguish "probability" per se from the normalized measure of the set (in the sense of Lebesgue) where the values of interest occur.

In a uniform medium of extinction σ_0,

$$\Pr(\mathrm{d}\sigma) = \delta(\sigma - \sigma_0)\mathrm{d}\sigma. \tag{59}$$

As a simple example of a variable medium, take a Bernoulli (binary-value) random extinction

$$\Pr(\mathrm{d}\sigma) = [f_1\delta(\sigma - \sigma_1) + f_2\delta(\sigma - \sigma_2)]\mathrm{d}\sigma, \ \ f_1 + f_2 = 1. \tag{60}$$

We will however usually be dealing with continuous distributions of σ, hence the differential notation.

"Ensemble" averages over this "disorder" in the optical medium will be denoted by angular brackets, $\langle\cdot\rangle$; so, for instance, we have

$$\langle\sigma^q\rangle = \int_0^\infty \sigma^q \Pr(\mathrm{d}\sigma). \tag{61}$$

Statistical quantities of interest in photon transport are the ensemble-averaged moments of the (random) FPD, equivalently, the moments of the ensemble-average FPD

$$\langle p(s)\rangle = \langle \mathrm{d}P(s)\rangle/\mathrm{d}s. \tag{62}$$

Specifically, we may want

$$\langle\mathcal{E}(s^q)\rangle = \int_0^\infty s^q \langle \mathrm{d}P(s)\rangle \tag{63}$$

where

$$\langle \mathrm{d}P(s)\rangle/\mathrm{d}s = \int_0^\infty p(s|\sigma)\Pr(\mathrm{d}\sigma) = \int_0^\infty \sigma\exp[-\sigma s]\Pr(\mathrm{d}\sigma). \tag{64}$$

So (63) is actually a double integral on probability measures: first on the spatial disorder, then on the propagation (as written above), or vice-versa.

Thinking of

$$\tau(s) = \sigma s \tag{65}$$

when extinction σ is random and distance s fixed, we are interested in the statistical properties of the mean direct transmission law

$$\langle \mathrm{e}^{-\tau(s)}\rangle = \int_0^\infty T_{\mathrm{dir}}(s|\sigma)\Pr(\mathrm{d}\sigma) = \int_0^\infty \exp[-\sigma s]\Pr(\mathrm{d}\sigma). \tag{66}$$

In short, how does it differ from $\mathrm{e}^{-\langle\tau(s)\rangle} = \mathrm{e}^{-\langle\sigma\rangle s}$? From (66), we recover the mean FPD in (64):

$$\langle \mathrm{d}P(s)\rangle = \left|\frac{\mathrm{d}}{\mathrm{d}s}\langle \mathrm{e}^{-\tau(s)}\rangle\right| \mathrm{d}s. \tag{67}$$

Three general results can be derived about the mean or "effective" FPD in (64) or (66)–(67).

1. It is exponential *only* if the medium is homogeneous, a consequence of Jensen's inequality for $f(X) = \mathrm{e}^{-X}$. This is the converse of the result derived in (43), thus making exactly exponential transmission and homogeneity equivalent statements about an optical medium:

$$\sigma(\boldsymbol{x}) \equiv \text{constant} \Longleftrightarrow \left|\frac{\mathrm{d}}{\mathrm{d}s}T_{\mathrm{dir}}\right| \propto T_{\mathrm{dir}}. \tag{68}$$

   An important corollary here is that effective medium (or homogenization) theory is of limited value as an approach for 3D RT in the presence of unresolved spatial variability. It is probably wise to customize the effective parameters of the uniform medium to deliver on some important aspect of the problem at hand, rather than to think of it as a truly "equivalent" medium.
2. The mean MFP is always larger than in the hypothetical homogeneous medium with an extinction equal to the mean extinction; considering (10), we are thus putting a number/mass-conservation constraint on the variability. This translates to

$$\langle \ell\rangle = \langle \mathcal{E}(s)\rangle = \langle 1/\sigma\rangle \geq 1/\langle\sigma\rangle. \tag{69}$$

   The inequality follows from Jensen's in (57) for the convex function $f(X) = 1/X$. The local quantity $1/\sigma(\boldsymbol{x})$ is probably not equal to the MFP defined in (50) for any direction $\boldsymbol{\Omega}$. However, it is clearly a better guess than the mean extinction $\langle\sigma\rangle$. I will call the local quantity $1/\sigma(\boldsymbol{x})$ the *pseudo*-MFP.
3. The mean FPD is always wider-than-exponential in the sense that its higher-order moments are always under-estimated by assuming an exponential distribution, even if we make a judicious adjustment for item 2 by using the actual MFP:

$$\langle \mathcal{E}(s^q)\rangle = \Gamma(q+1)\langle\sigma^{-q}\rangle \geq \Gamma(q+1)\langle\sigma^{-1}\rangle^q = \Gamma(q+1)\langle\ell\rangle^q,\ q > 1. \tag{70}$$

   This follows from Jensen's inequality for $f(X) = X^q$ for $q > 1$, which is also true for[6] $-1 < q < 0$ (as a means of emphasizing small s values rather than large ones).

General proofs draw on characteristic-function theory in probability [28]; see Davis and Marshak [27] for details. Figure 3 illustrates the three results with the simple Bernoulli variability model in (60), noting that no account is taken (yet) for correlation lengths as in stochastic RT in Markovian Media.

[6] For moments of order $q \leq -1$, the PDF (of $X = 1/\sigma$ in this case) must vanish sufficiently fast at 0.

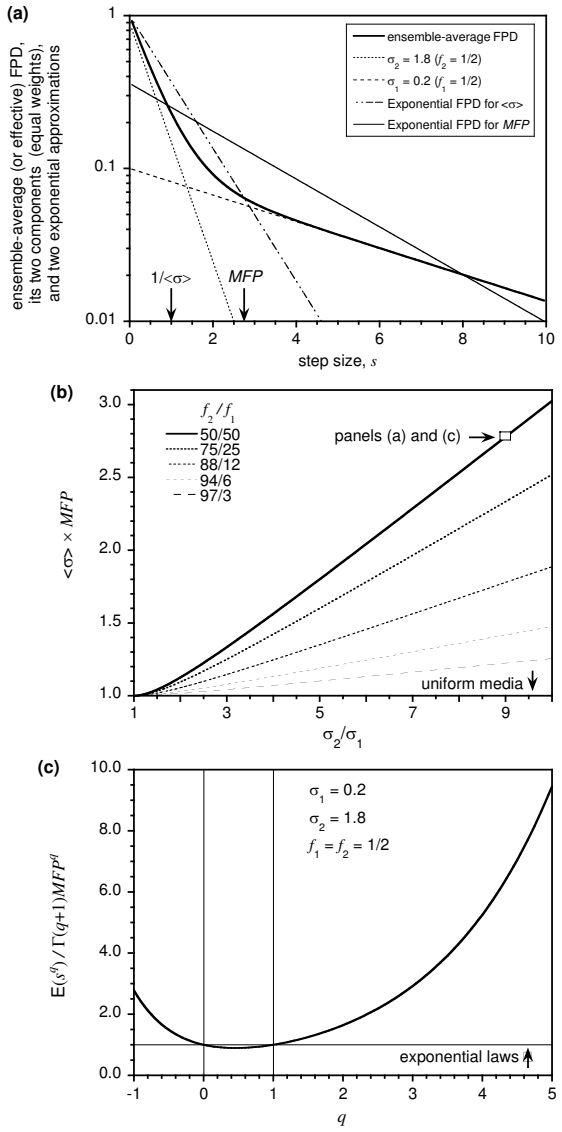

Fig. 3. Remarkable inequalities for propagation in a binary mixture of extinctions, before correlations are considered. **(a)** The actual FPD is compared with its two exponential components for $\sigma_1 = 0.2$ and $\sigma_2 = 1.8$ with $f_1 = f_2 = 1/2$ in (60); the short steps are dominated by the dense half and the long ones be the tenuous half. Two exponential approximations based on $\langle\sigma\rangle = f_1\sigma_1 + f_2\sigma_2 = 1$ and on the actual MFP $\langle 1/\sigma\rangle = f_1/\sigma_1 + f_2/\sigma_2 = 2.77\cdots$ are also plotted. **(b)** The actual MFP is compared to the prediction $1/\langle\sigma\rangle$ based on mean extinction as σ_2/σ_1 increases from 1 to 10 and as the mixing ratio f_2/f_1 varies; the special case used in panels (a) and (c) is highlighted. **(c)** Statistical moments $\mathcal{E}(s^q)$ of the actual FPD are compared with the exponential prediction $\Gamma(q+1)\langle 1/\sigma\rangle^q$ based on the actual MFP. The underestimation of moments at both higher-order ($q > 1$) and negative order ($q < 0$) is a direct consequence of the wider-than-exponential nature of the actual FPD. Note that, although their plotted ratio is finite, both moments are in fact divergent for $q \leq -1$. Adapted from Fig. 1 in [27]

The Key Role of Spatial Correlations

What is the point of the mathematical exercise summarized in the previous subsection? What makes an average of the FPD over an ensemble of extinction values relevant to 3D RT? Can we dismiss the strong corollary that limits the scope of effective medium theory? These questions can only be addressed by considering the spatial correlations of the random field $\sigma(\boldsymbol{x})$. Indeed, recalling that Ξ is the unit sphere, we really should have started with

$$\Pr(\mathrm{d}\tau|s) = \Pr\{\boldsymbol{x} \in \mathrm{M}, \boldsymbol{\Omega} \in \Xi :\ \tau \leq \int_0^s \sigma(\boldsymbol{x} + \boldsymbol{\Omega}s')\mathrm{d}s' < \tau + d\tau\} \tag{71}$$

for the variability of optical distance over a given physical distance s, rather than (58).

Implicitly, we have assumed that the development from Eq. (58) to Fig. 3 applies to

$$\overline{\sigma}_s(\boldsymbol{x}, \boldsymbol{\Omega}) = \tau(s; \boldsymbol{x}, \boldsymbol{\Omega})/s = \frac{1}{s}\int_0^s \sigma(\boldsymbol{x} + \boldsymbol{\Omega}s')\mathrm{d}s', \tag{72}$$

where we used the definition in (40) and introduce an over-score to denote line-averaged quantities.[7] This is just the line-average of $\sigma(\boldsymbol{x})$ along a finite portion of the beam $\{\boldsymbol{x}, \boldsymbol{\Omega}\}$. Note that

$$\overline{\sigma}_0(\boldsymbol{x}, \boldsymbol{\Omega}) \equiv \sigma(\boldsymbol{x}),\ \forall \boldsymbol{\Omega}, \tag{73}$$

as long as $\sigma(\boldsymbol{x})$ has some degree of continuity, i.e., that the local Hölder (a.k.a. regularity) exponent $h(\boldsymbol{x})$ in

$$|\sigma(\boldsymbol{x} + \boldsymbol{r}) - \sigma(\boldsymbol{x})| \sim r^{h(\boldsymbol{x})} \tag{74}$$

verifies $h(\boldsymbol{x}) > 0$ almost everywhere.

Apart from somewhat heavier notations, the arguments of Sect. 3.4 leading to the inequalities in (69)–(70) carry over to $\overline{\sigma}_s$, as a random field with statistical properties that will generally depend parametrically on s. However, the equalities expressed in formulas (69) and (70) to the left of the "$\geq$" carry over as good approximations only if we add one extra condition. Specifically, we require that the 1-point statistics (i.e., PDFs) of $\overline{\sigma}_s$ depend only weakly on s over a significant range of s-values starting of course at 0. As it turns out, this *mandates* that the extinction field has correlations over that same range of scales, at least in its 2-point statistics such as the (2nd-order) structure function, $\langle[\sigma(\boldsymbol{x} + \boldsymbol{r}) - \sigma(\boldsymbol{x})]^2\rangle$ where $\boldsymbol{r}$, is a given displacement vector. See the appendix in Davis and Marshak [27], with A. Benassi, for a detailed proof.

This is just a formal way of making a quite natural assumption, one that all instrument designers make to some extent for the purposes of signal-to-noise management. We are simply saying that a (less noisy) estimate of a spatial average is almost as good as a quasi-point-wise value, only with some tolerable (and maybe correctable) loss of extreme values. And this in turn requires that the optical medium has correlations over the range of scales for which (74) applies. As shown by Davis

[7] Recall that averages over the 3D disorder are denoted $\langle\cdot\rangle$ while averages over the photon transport are denoted $\mathcal{E}(\cdot)$.

and Marshak, the well-documented turbulent/fractal structure of terrestrial clouds guarantees that such correlations exist. Indeed, clouds are "scaling" in the sense that

$$\langle |\sigma(\boldsymbol{x}+\boldsymbol{r}) - \sigma(\boldsymbol{x})|^p \rangle \sim r^{\zeta(p)} \tag{75}$$

over a significant range of scales r (2 to 3 orders of magnitude at least). The l.-h. side of (75) is called the "pth-order structure function" and $\zeta(p)$ is known to be a continuous concave function as long as the dependance on p of the prefactors on the r.-h. side can be neglected (yet another consequence of Jensen's inequality). The exponents $\zeta(p)$ can in fact be obtained from the spatial/ensemble statistics of $h(\boldsymbol{x})$ in (74), and vice-versa, using Frisch and Parisi's [29] multifractal formalism. This kind of scaling is associated with long-range correlations and leads to a correspondingly weak dependence on s of the PDF of $\overline{\sigma}_s$ in (72); see Fig. 4 for computations based on synthetic turbulence data.

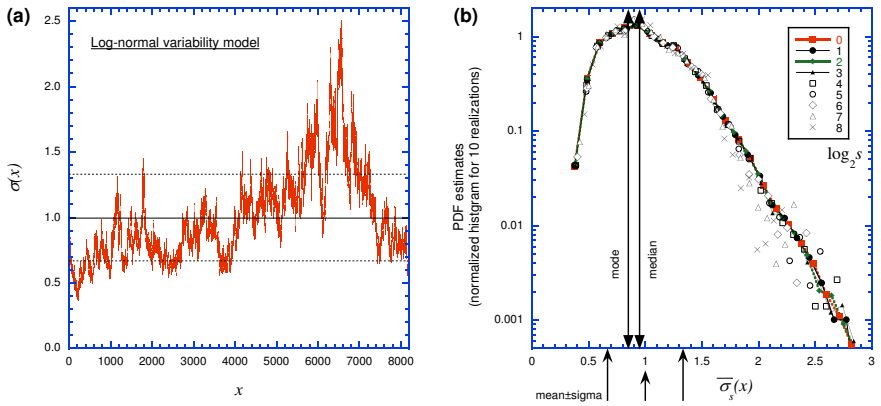

Fig. 4. Example of a transect through a random multifractal extinction field with lognormal statistics. This data is synthetic but the 1- and 2-point statistics are typical of in-cloud extinction variability [30] and such stochastic models are used routinely in 3D RT cloud studies. **(a)** Sample realization $\sigma(x)$ with a log-normal PDF generated by exponentiating fractional Brownian motion [31] with a wavenumber spectrum in $k^{-5/3}$; the mean (solid line) is set to unity and the std. dev. is $\pm 1/3$ (dashed lines). **(b)** Illustration of the "1-point scale-independence" property [27]: PDFs of segment averages $\overline{\sigma}_s(x)$ in (72) do not depend on segment length for all but the most extreme values. Adapted from Fig. 6 in [27]

That is not the end of the story. It is important to assess the resilience or fragility of Beer's exponential transmission law to perturbation by 3D variability. Under what conditions is the MFP significantly larger than $1/\langle\sigma\rangle$? And when are the qth-order

moments ($q > 1$) of s significantly larger than the prediction of the exponential distribution? Intuitively, this calls for two conditions:

1. that the amplitude of the 1-point variability is sufficient (cf. Fig. 3b);
2. that at least some of the scales of *correlated* 2-point variability are commensurate with the MFP.

In item 2, we are thinking about the *actual* MFP and not the biased estimate $1/\langle\sigma\rangle$. Recall that the actual MFP can become much larger than $1/\langle\sigma\rangle$ if there are significant regions of low extinction (consider Fig. 3b when σ_1 becomes very small).

Davis and Marshak call condition #2 "resonant" variability noting that it is a rather broad resonance, easily achieved in terrestrial clouds and cloud systems. So non-exponential transmission laws are expected to be the rule rather than the exception. Other situations can however arise, at least in theory. At a given amplitude, even quite large amplitude variability can be "too fast" or "too slow" to generate the interesting non-exponential transmission laws. To wit,

- if the extinction field is varying so fast that every photon can sample essentially all the variability between almost every scattering, emission or absorption event, then surely only the ensemble-mean extinction really matters because that is (to high accuracy) the outcome of (72);
- in contrast, if the extinction field varies so slowly that from its creation to its absorption, escape or detection each photon samples basically just one value of σ, then the ensemble-average transmission law is irrelevant to the transport.

The former is the too-fast scenario, a.k.a. the atomistic mix (in stochastic RT theory), and the pertinent approach to assess the bulk transport is to use the mean properties in a homogeneous computation. The latter is the too-slow scenario and an average over homogeneous multiple-scattering computations weighted by the 1-point statistics of the extinction field. This procedure is known in cloud radiation studies as the Independent Pixel/Column Approximation [32, 33].

Non-Poissonian Point-Process Approach

In this subsection, I adopt Kostinski's [26] perspective on extinction as a point process. I'll start with *uniform* optical media. Infinitesimal particles are distributed at random, uniformly in space, according to some density n. The photons in a given light beam interact with these particles simply where they are, so extinction events

1. are a statistically homogeneous process, i.e., which does not depend on position;
2. for small enough volumes, the probability of intercepting more than one photon is vanishingly small; and
3. events in non-overlapping volumes are statistically independent.

These properties define a Poisson point-process [34]. So the discrete probability of obtaining exactly $N \geq 0$ photon interactions (extinction events) over a given distance s is

$$p_N(s;m) = p_N(m) = \frac{m^N}{N!} \times \mathrm{e}^{-m} \tag{76}$$

where the sole parameter is the mean of N at given s,

$$m = \mathcal{E}(N|s). \tag{77}$$

The variance $\mathcal{D}(N|s)$, defined as in (56), of a Poisson deviate is equal to its mean.[8] We also re-emphasize that, since we are averaging here over the photon transfer events, we use the notation with $\mathcal{E}(\cdot)$'s.

Now, setting $N = 0$ (no events whatsoever over the segment of given length s), we get $p_0(s) = \exp(-m)$. By definition, this is direct transmission $T_{\rm dir}(s)$. We can therefore make the identification

$$m = \tau(s) = \sigma s \tag{78}$$

in (43), recalling that we found σ (in this case constant) to be particle density n times the collision cross-section per particle $\mathtt{s}$. This is reminiscent of the interpretation of optical distance $\tau(s)$ as distance s in units of MFPs; more precisely here, $\tau(s)$ is the average number of collisions m suffered over distance s, at the average rate of one per MFP. Of course, at the single photon level, only one such interaction is enough to remove it from the beam, however, a small number of lucky ones can travel across large (optical) distances, that is, several MFPs.

We now turn to "lumpiness" in *non-uniform* optical media, translating to spatial correlations between the particles, hence between the extinction events. In point process theory, correlation is defined as the deviation from Poissonian behavior in the joint probability of finding exactly one particle in each of two small volumes δV_1 and δV_2 at a distance r:

$$\Pr\{N_1 = N_2 = 1; n, r\} = n^2 \delta V_1 \delta V_2 [1 + \eta(r)] \tag{79}$$

where n is the *mean* density of the particles. Because of their independence in a uniformly random medium, the Poissonian prediction is $\eta(r) = 0$ while $\eta(r) \neq 0$ corresponds to some kind of particle correlation in the medium. In short, we retain above properties #1 and #2 but relax #3.

Another, more practical, way of defining $\eta(r)$ uses the "pair correlation" $\langle N(0)N(r)\rangle$. We have

$$\eta(r) = \langle N(0)N(r)\rangle / \langle N\rangle^2 - 1 \tag{80}$$

where N is the number of particles in the small[9] test volume δV. We have $\langle N\rangle = n\delta V$ and we consider two such volumes at a distance r. If the events $N(0)$ and $N(r)$ are independent, then $\langle N(0)N(r)\rangle = \langle N(0)\rangle\langle N(r)\rangle = \langle N\rangle^2$, hence $\eta(r) = 0$. Note that, as in (61), we are averaging here over the disorder of the particle distribution, hence the use of $\langle\cdot\rangle$'s.

Following Landau and Lifschitz's [35] general analysis of fluctuations and correlations in gases and liquids near a phase transition, it can be shown that, in a small test volume δV, one has

$$\langle \delta N^2\rangle = \langle N\rangle + \overline{\eta}\langle N\rangle^2 \tag{81}$$

where $\delta N = N - \langle N\rangle$ and $\overline{\eta}$ is the volume average of $\eta(r)$ over δV. For example, we have

$$\overline{\eta}(r) = \frac{3}{r^3}\int_0^r r'^2 \eta(r')\mathrm{d}r' \tag{82}$$

---

[8] This might sound dissonant to some readers on dimensional grounds. (Should that not be standard deviation $= \sqrt{\mathcal{D}}$? That is until we recall that this random variable is a pure number: we are just counting events.

[9] As $n\delta V$ becomes small, we have $N = 0, 1$ depending on whether a particle is present or not, the former becoming the dominant event as soon as $n\delta V \ll 1$.

with $r = \sqrt[3]{3\delta V/4\pi}$ in the case of a spherical volume. Any deviation of $\overline{\eta}$ from 0 in (81) takes event variance $\langle \delta N^2 \rangle$ away from the Poissonian value of $\langle N \rangle$.

Returning to photon transport through a particulate medium, how do we now estimate $p_N(s)$ in the presence of spatial correlations? Kostinski proposes to use Mandel's formula from statistical optics [36]:

$$\langle p_N(s) \rangle = \int_0^\infty p_N(s|m) \Pr(\mathrm{d}m) = \frac{1}{N!} \int_0^\infty m^N \mathrm{e}^{-m} \Pr(\mathrm{d}m) \tag{83}$$

where $\Pr(\mathrm{d}m)$ is the element of probability that the sole parameter of the (discrete) Poissonian distribution in (76), now a (continuous) random variable, falls between m and $m + \mathrm{d}m$. Accordingly, we have transmuted the ";" separator into a "|" in the argument of p_N under the first integral.

For $N = 0$, this is equivalent to the computation of $\langle \mathrm{e}^{-\tau(s)} \rangle = \int \exp(-\tau) \Pr(\mathrm{d}\tau|s)$ in (66) since τ is also equal to $m = \sigma s$, σ being the random quantity at present. So the three general properties of $\langle \mathrm{e}^{-\tau(s)} \rangle$ and its derived quantities stated in Sect. 3.4 will follow from this alternative model for photon transport.

The close formal analogy between (66) and (83) is traceable to the close connection between collision statistics, (direct) transmission, and FPDs. The essential difference between the continuum transport-theoretical and random point-process approaches is that, coming from the latter less-familiar perspective, the question of spatial correlations (i.e., droplet clumping tendencies) arises immediately, at any rate, *before* the question of how to average over the spatial disorder. In the more familiar continuum approach, we first argued for averaging the (partial) kernel and then argued that the outcome, as strikingly different as it is from an exponential, is only relevant if the optical medium has spatial correlations that overlap with the MFP. The central role of the MFP is not that obvious in the point-process framework.

3.5 Results for Gamma-Distributed Extinctions, and Point-Process Equivalents

We assume here a Gamma-distribution for $\tau = m$ in (83) or, equivalently, for $\tau = \sigma s$ in (64) at a given distance s. The two parameters of this distribution are the mean, $\langle \sigma \rangle s$, and[10]

$$a = \frac{\langle \tau(s) \rangle^2}{\langle (\tau(s) - \langle \tau(s) \rangle)^2 \rangle} = \begin{cases} \langle \sigma \rangle^2 / \langle (\sigma - \langle \sigma \rangle)^2 \rangle & \text{in the continuum approach} \\ \langle m \rangle^2 / \langle (m - \langle m \rangle)^2 \rangle & \text{in the point-process approach} \end{cases} \tag{84}$$

where we recognize a variance in the denominator. So the degenerate (uniform extinction, Poissonian events) case is retrieved in the limit $a \to \infty$: as in (59), no variance at all. The PDF for $\tau(s)$, hence for m, reads as

$$\Pr(\mathrm{d}\tau|s) = p(\tau; \langle \sigma \rangle s, a)\, \mathrm{d}\tau = \frac{1}{\Gamma(a)} \left(\frac{a}{\langle \sigma \rangle s} \right)^a \times \tau^{a-1} \exp[-a\tau / \langle \sigma \rangle s]\, \mathrm{d}\tau. \tag{85}$$

[10] a is the squared inverse of the standard non-dimensional variability parameter, i.e., std.-dev./mean.

The second argument —and first parameter— is the mean of $\tau(s)$. By writing it as $\langle\sigma\rangle s$ the *given* step size s appears. The Gamma-distribution has the exponential (or Laplace) law of extinction variability as a special case when $a = 1$:

$$\Pr(\mathrm{d}\tau|s) = p(\tau;\langle\sigma\rangle s, 1)\mathrm{d}\tau = \exp[-\tau/\langle\sigma\rangle s]\mathrm{d}\tau/\langle\sigma\rangle s, \tag{86}$$

not to be confused with (Beer's) exponential law of direct transmission. As another example, reconsider Figs. 4 where we see a synthetic in-cloud variability with $a = 9$ in (84), a reasonable amount of skewness (log-normal PDF), and realistic 2-point correlations (associated with the prescribed $k^{-5/3}$ wavenumber spectrum).

The above choice of variability model for $\tau(s)$ is not arbitrary. We have adopted the convenient as well as reasonably accurate parameterization by Barker et al. [37] of the observed variability of optical depth (measured vertically) in high-resolution satellite images of a wide variety of cloud scenes. Figure 5 reproduces their evidence for Gamma-distributions for $\tau(s)$, where s is the thickness of the cloud layer using LandSat imagery with ≈30 m pixels and ≈60 km swaths. We note that Barker et al.'s determination of cloud optical depth for each LandSat pixel is based, as usual in cloud remote sensing, on a 1D RT model and this procedure is known to underestimate the variance [38]; so the inferred values of a are likely to be upper bounds.

In the continuum approach from Sect. 3.4, this choice of variability model applied to (66) yields

$$\langle T_{\mathrm{dir}}\rangle(s;\langle\sigma\rangle, a) = \langle \mathrm{e}^{-\tau(s)}\rangle = \frac{1}{(1+\langle\sigma\rangle s/a)^a} \tag{87}$$

for the mean transmission law which is plotted in Fig. 6b. As expected, the exponential law $\exp(-\langle\sigma\rangle s)$ is recovered (using L'Hôpital's rule) in the degenerate-σ limit $a \to \infty$. Otherwise, direct transmission is effectively power-law, with diverging moments $\langle\mathcal{E}(s^q)\rangle$ for $q \geq a$. Assuming $a > 1$, the MFP exists and is given by

$$\langle\mathcal{E}(s)\rangle = \langle\sigma^{-1}\rangle = \left(\frac{a}{a-1}\right)\langle\sigma\rangle^{-1}. \tag{88}$$

Notice the excess over the standard prediction using $\langle\sigma\rangle^{-1}$. It is easy to verify here the general result that $\langle\mathcal{E}(s)\rangle = \langle 1/\sigma\rangle$ using the PDF in (85).

In the discrete point-process approach from Sect. 3.4, the same choice of variability in Eq. (85) now reads as

$$\Pr(\mathrm{d}m|s) = p(m;\langle\sigma\rangle s, a)\mathrm{d}m = \frac{1}{\Gamma(a)}\left(\frac{a}{\langle\sigma\rangle s}\right)^a \times m^{a-1}\exp[-am/\langle\sigma\rangle s]\mathrm{d}m \tag{89}$$

where $\langle\sigma\rangle s = \langle m\rangle$. Applying this to (83) leads to a so-called negative binomial distribution for N. More precisely, we have

$$\langle p_N(s)\rangle = p_N(\langle\sigma\rangle s, a) = \frac{(\langle\sigma\rangle s)^N}{N!} \times \frac{\Gamma(N+a)}{\Gamma(a)(a+\langle\sigma\rangle s)^N} \times \frac{1}{(1+\langle\sigma\rangle s/a)^a}. \tag{90}$$

The case $a \in \mathbb{N} - \{0\} = \{1, 2, \ldots\}$ is known as the Pascal distribution and it arises naturally from the theory of Bernoulli processes. Specifically, the question is about the probability of having exactly $a \geq 1$ successes with probability p and $N \geq 0$ failures with probability $q = 1-p$, ending with a success, when $p = 1/(1+\langle\sigma\rangle s/a) \leq 1$. Equation (90) can thus be expressed formally as

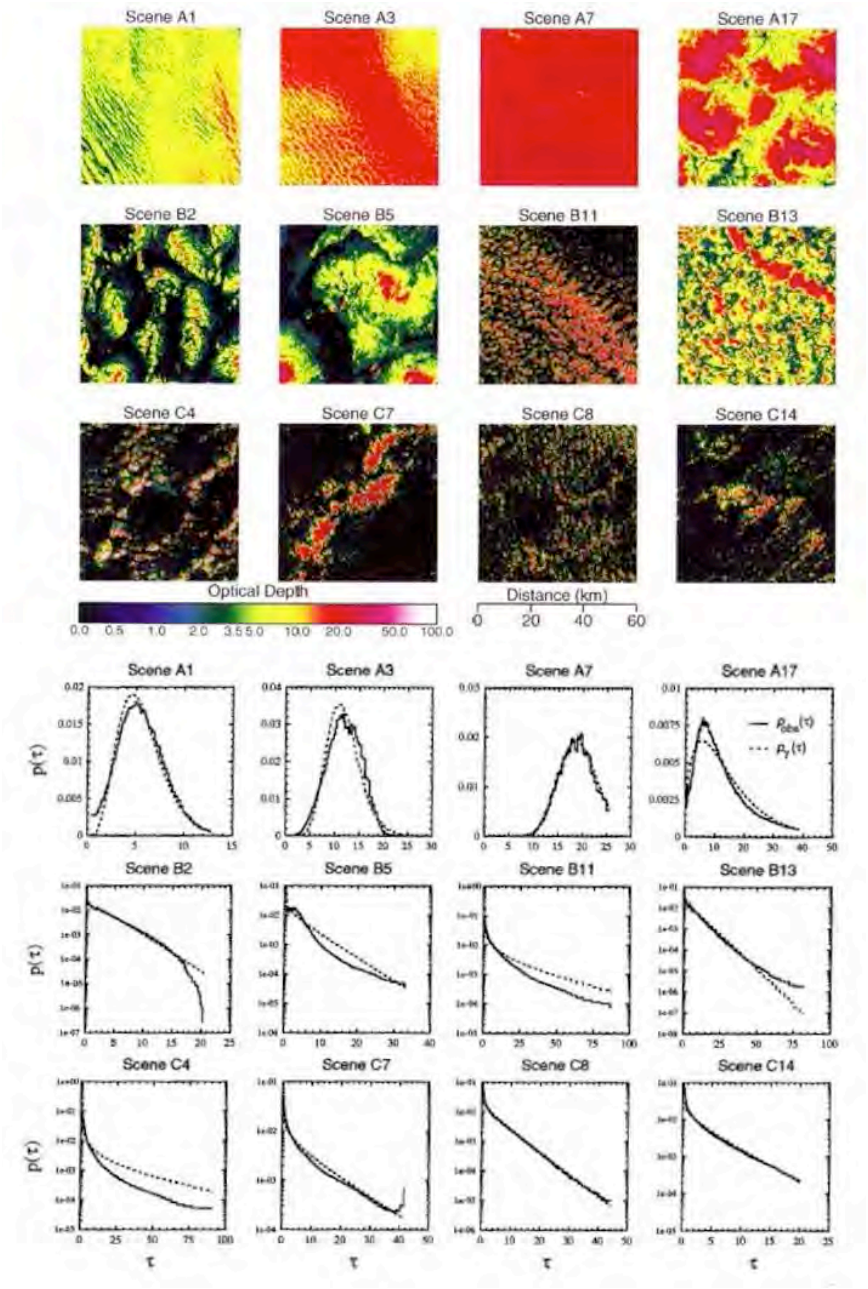

Fig. 5. Empirical support for Gamma-distributed extinction variability in the Earth's cloudy atmosphere, reproduced from Figs. 1–2 in [37] with permission. **(above)** Cloud optical depth fields retrieved from more or less cloudy LandSat images: upper row, very cloudy ($1.6 \lesssim a \lesssim 22.5$); middle row, partially cloudy ($0.4 \lesssim a \lesssim 1.3$); lower row, sparse clouds ($0.2 \lesssim a \lesssim 0.8$). Note that optical depth is proportional to extinction averaged vertically over the thickness of the cloud layer. **(below)** The inferred Gamma distributions (in one-to-one correspondence with the above images) are generally in good agreement for the whole optical depth PDF: observed histograms in solid lines; Gamma-PDF predictions (based only the observed mean and variance) in dashed lines. Figure 6a illustrates in more detail the whole family of Gamma distributions.

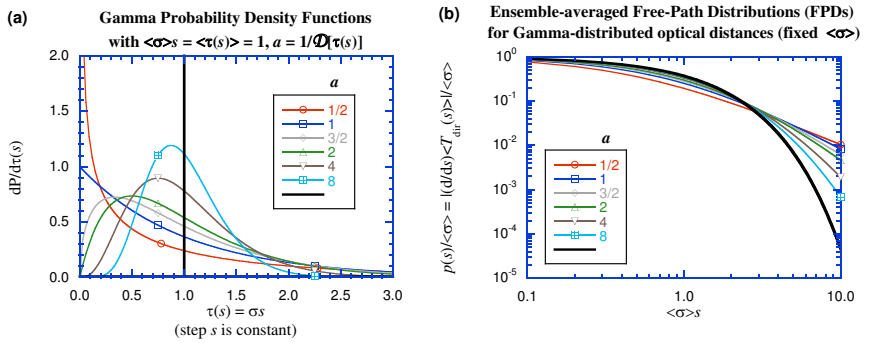

Fig. 6. Gamma-distributed optical distances for a given physical distance: **(a)** PDFs of τ from (85) for a given s and selected variability parameters, **(b)** the resulting mean transmission laws from (87) plotted in log-log axes to highlight the power-law tails

$$\langle p_N(s)\rangle = (-1)^N \binom{-a}{N} \times \left(\frac{\langle\sigma\rangle s}{a+\langle\sigma\rangle s}\right)^N \times \frac{1}{(1+\langle\sigma\rangle s/a)^a} \tag{91}$$

even if $a > 0$ is non-integer.[11]

For $N = 0$, we naturally find the same non-exponential transmission laws as in (87) and Fig. 6b. However, looking back at (49), where we assumed $a = M \gg 1$ for a fixed value of $\langle\sigma\rangle s$, we can interpret "success" probability $p = 1/(1+\langle\sigma\rangle s/a) \approx 1 - \langle\sigma\rangle s/a$ as that of a particle being transmitted through the $1/a$th part of s for a given $\langle\sigma\rangle$. Thus, for $N = 0$ "failures" to be transmitted a successive times through that ath portion of optical distance $\langle\sigma\rangle s$, we indeed find (87) for the direct transmission. So clearly the most interesting situation is when $a \approx \langle\sigma\rangle s$, i.e., when any given *physical* distance s is divided roughly into as many distinguishable parts or "clumps" as its (mean) value in *optical* units.

The mean of N is still $\mathcal{E}(N) = \langle\sigma\rangle s$ in (90). Mimicking the form of (81) to emphasize the relation to pair-correlations, we find for the variance of N

$$\mathcal{D}(N) = \mathcal{E}(\delta N^2) = \mathcal{E}(N) + \overline{\eta}\mathcal{E}(N)^2 \tag{92}$$

where $\delta N = N - \mathcal{E}(N)$ with

$$\overline{\eta} = 1/a \geq 0. \tag{93}$$

Accordingly, $\langle p_N(s)\rangle$ in (90) is sometimes called the "over-dispersed" Poisson distribution. It is nonetheless remarkable that in (93) the point-process approach ties the 2-point statistical quantity $\overline{\eta}$ in (81) and the 1-point statistical variability parameter a from (84). In density-based stochastic modeling, one can generally choose the PDF and the correlation structure independently.

[11] The usual binomial coefficients $\binom{n}{i}$ are defined by the identity $(p+q)^n = \sum_{i=0}^{n}\binom{n}{i}p^{n-i}q^i$ where $p+q=1$ in the well-known application to combinatorics; "negative" binomial coefficients are defined by the identity $(1-q)^{-r} = \sum_{i=0}^{\infty}\binom{-r}{i}(-q)^i$ for $r > 0$.

The above results generalize at once the Poissonian ($a = \infty$, $\mathcal{D}(N) = \mathcal{E}(N)$) case in (76) with $m = \langle\sigma\rangle s$ and the $a = 1$ case in (86) that was used by Kostinski [26] as a rather extreme example of sub-exponential transmission:

$$\langle T_{\rm dir}\rangle(s;\langle\sigma\rangle,1) = p_0(\langle\sigma\rangle s,1) = \frac{1}{1+\langle\sigma\rangle s}. \tag{94}$$

This is indeed the critical value of a at which the MFP becomes (logarithmically) divergent and it hails from the special case of (90) with $a = 1$ known as the geometric distribution,

$$p_N(\langle\sigma\rangle s,1) = \left(\frac{\langle\sigma\rangle s}{1+\langle\sigma\rangle s}\right)^N \times \frac{1}{1+\langle\sigma\rangle s}. \tag{95}$$

That is the probability of exactly $N \geq 0$ failures before one success when each Bernoulli event is a success with probability $p = \langle T_{\rm dir}\rangle = (1+\langle\sigma\rangle s)^{-1}$ in (94).

3.6 From Positive to Negative Correlations

Physically, what is it about the spatial correlations that is causing the systematic deviations from exponential transmission? Even if there is a single direction of propagation, we are always computing a projection of the particle-light interaction cross-sections parallel to the beam (cf. Fig. 1). There is naturally random overlap in these projections. What the spatial correlations effectively do is to cause *more* overlap in the projections, hence *more* photons are transmitted. The sub-exponential laws we found above are the statistical consequence of this clustering.

From there, it is of interest to consider the possibility of *negative* correlations in the spatial fluctuations of the extinction field (in the continuum approach) or in the pair-correlation function (in the point-process approach). In the extinction field picture, this means that a fluctuation above the mean is more likely than not to be very quickly followed by a fluctuation below the mean, and vice versa; in a sense, this is "fast" variability with a tendency to overshoot the mean. In the pair-correlation picture, this means that the scattering/absorbing particles essentially repel each other, leading to even more uniformity in space than obtained by random (Poisson) positions. The outcome in (80) is $\eta(r) < 0$ at least for small values of point-separation distance r. From there, $\overline{\eta}(r)$ in (81)–(82) will also be < 0, at least for small enough $\delta V(r) = (4\pi/3)r^3$.

What are the consequences of negative correlations for photon transmission? Shaw et al. [39] use the pair-correlation model to show that a super-exponential (faster-than-exponential) transmission law will follow from $\eta(r) < 0$. The continuum approach has more trouble here because negative correlations are just different incarnations of the uniform-σ hypothesis.

The question of how relevant negatively-correlated media are to atmospheric optics is, at present, entirely open [27]. The balance of evidence however favors further consideration of the positive correlations related to droplet or cloud clustering. The known mechanisms that cause cloud particles to repel each other, as listed by Shaw et al. [39], indeed require either very close proximity (threatening the important dilution requirement in any transport theory based on geometric optics) or else rather unusual circumstances (e.g., still air, electric charge separation). Negative correlations can occur also at macroscopic scales: certain types of cloud layers (e.g., marine stratocumulus) are systematically topped by clear layers, trains of orographic clouds

downwind from a mountain range will also yield negative correlations at regular distances. However, in both these cases, any chance of occurrence of another cloud further along in the vertical or horizontal direction will restore positive correlations, which already dominate at the micro-scale.

3.7 Summary, Discussion, and Outlook

On the one hand, we have established the deep non-Poissonian nature of photon transport in variable optical media and, on the other hand, we have underscored the importance of having spatial correlations over MFP scales to obtain non-exponential FPDs. An inescapable consequence of deviations from spatial uniformity of the cloud droplets is that the mean (or effective) photon transport kernel is non-exponential. More precisely it is sub-exponential in the case of positive correlations (clumping tendencies).

In the atmosphere, spatial correlations in cloud structure exist over a vast range of scales horizontally as well as vertically, although clearly in qualitatively different ways. This range goes from centimeters at least up to the thickness of the troposphere ($\approx$10 km), and often much more in the horizontal. There are both positive and negative correlations, but at scales that matter for photon transport they are overwhelmingly positive.

Two-point spatial correlations, even of the right sign and over the right range of scales, are of little consequence unless extinction (and, hence, the pseudo-MFP) also vary widely enough in the sense of the 1-point statistics (i.e., the PDF). Consider the following two scenarios:

- In a single dense un-broken cloud layer, the MFP is small with respect to the physical thickness of the layer. This is equivalent to saying that the layer is optically thick and that (literally) an exponentially small amount of direct sunlight gets through.
- Now imagine a complex situation with broken clouds and possibly also multiple layers (not necessarily all optically thick), and add to that a partially reflective surface. In this case, the optical quasi-vacuum between the clouds dominates the average $\langle 1/\sigma \rangle$ of the local pseudo-MFP. So this estimate of the overall MFP can be huge, possibly larger than the physical thickness of the whole cloudy region. In particular, abundant direct sunlight can reach the ground in spite of the presence of clouds.

In the following section, we will see that

- in the former case, radiation is transported by standard diffusion, each photon executes a convoluted trajectory. This path is a classical (Gaussian) random walk with an inner cut-off at the small MFP scale and an outer cut-off determined by the finite thickness of the cloud layer.
- in the later case, radiation is transported by anomalous diffusion where most steps in the random walk (inside clouds) are small but some steps (between clouds and/or surface) can be huge. This is as predicted by the basic transport computations presented above in the presence of positive correlations and, in this case, the photons execute Lévy-type random walks [40] where the tail of the step distribution is power-law.

Before moving on, we note that Borovoi [41] objected to Kostinski's [26] linkage of non-Poissonian droplet distributions and sub-exponential transmission laws in the light of his previous [42] investigation that used standard transport theory and favored effective medium theory (hence *modified* exponential transmission laws). Kostinski's reply [43] is worth reading in that it (1) reasserts the relevance of the spatial correlations, and hence of non-exponential transmission laws, and (2) claims that the point-process model is more general than standard transport theory because it allows for negative correlations. In [27], we agree with Kostinski on the former claim, coming from the transport theoretical perspective used by Borovoi (cf. Sects. 3.4–3.4), but we have reservations about the latter claim. First, the atmospheric scenarios for negative correlations are marginal if not implausible (as argued above); secondly, empirical evidence weighs in for sub-exponential transmission laws (cf. Sect. 5); thirdly, I have unpublished results showing that density-based computations can handle negative correlations and lead to super-exponential transmission laws (the variability of course has to violate the continuity conditions required in the above). Most importantly however, the author views this as a healthy debate on the fundamentals of 3D RT.

4 Multiple Scattering and Diffusions

4.1 Multiple Forward Scatterings

Let $\mathbf{\Omega}_0$ be the initial direction of propagation in $\mathbb{R}^3$, or position on Ξ, for a particle beam in a medium with conservative ($\varpi_0 = 1$) axi-symmetric scatters. The medium may be variable but we will assume the scattering phase function is the same everywhere. By symmetry, the average direction $\mathcal{E}(\mathbf{\Omega}_n)$ is $\mathbf{\Omega}_0$ for any number of scatterings n. By taking $\mathbf{\Omega}_0$ as the polar axis ($\mu_0 = 1$), we can use $\theta_n = \cos^{-1}(\mathbf{\Omega}_0 \bullet \mathbf{\Omega}_n) = \cos^{-1}(\mu_n)$ to measure the (great-circle) distance on Ξ between initial and current directions of propagation.

From (29), we know that

$$\mathcal{E}(\mathbf{\Omega}_0 \bullet \mathbf{\Omega}_1) = \ldots = \mathcal{E}(\mathbf{\Omega}_{n-1} \bullet \mathbf{\Omega}_n) = g \in [-1, +1]. \tag{96}$$

I now show by induction that

$$\mathcal{E}(\mu_n) = \mathcal{E}(\mathbf{\Omega}_0 \bullet \mathbf{\Omega}_n) = g^n. \tag{97}$$

Indeed, the only component of interest is $(\Omega_z)_n = \mu_n$; all others vanish upon averaging, by symmetry. From spherical trigonometry,

$$\mu_{n+1} = \mu_n \mu_\mathrm{s} + \sqrt{1-\mu_n^2}\sqrt{1-\mu_\mathrm{s}^2}\cos\phi_\mathrm{s} \tag{98}$$

where the azimuthal angle ϕ_s in the second term is uniformly distributed on [0,2π) and uncorrelated to θ_s and θ_n; so it averages to zero. Therefore $\mathcal{E}(\mu_{n+1}) = \mathcal{E}(\mu_n \mu_\mathrm{s})$. Like in the propagation part of particle transport, there is a (discrete) Markovian property for scattering: transition probability is independent of present state. This leads to[12]

[12] An interesting corollary of this recursion formula is that, if the phase function is Henyey–Greenstein, then the angular distribution of n-times scattered radiance

$$\mathcal{E}(\mu_{n+1}) = \mathcal{E}(\mu_n)\mathcal{E}(\mu_\mathrm{s}) = \mathcal{E}(\mu_n)g,\ \forall n, \tag{99}$$

and thus completes the proof.

Equation (97) enables us to quantify accurately the decay of directionality in a light beam embedded deeply in a uniform turbid medium, sometimes called "blooming:" $\mathbf{\Omega}_n$ can be anywhere on Ξ with almost equal probability as soon as we have, say, $\mathcal{E}(\mu_n) \approx 1/\mathrm{e}$. This happens at a critical scattering order $n^* \approx -1/(\ln g)$. For small enough values of $(1-g)$, this reads as

$$n^* \approx 1/(1-g) \tag{100}$$

which roughly defines the number of forward-peaked scattering events required for the photon to loose almost all memory of its original direction of travel. Another way of showing that directional memory is short (i.e., lost in finite time) is to view the typical great-circle distance from the origin, $\theta_n = \cos^{-1}\mu_n$, as a discrete-time diffusion on the sphere. By identifying $\mathcal{E}[\cos\theta_n] \approx 1-\mathcal{E}[\theta_n^2]/2$ on the tangent plane[13] of Ξ at $\mu = 1$ and, remarking that $g^n = [1-(1-g)]^n \approx 1-n\times(1-g)$ when $(1-g) \ll 1$, we obtain

$$\mathcal{E}[\theta_n^2] \approx 2(1-g)n. \tag{101}$$

So $2(1-g)$ plays the role of a diffusivity constant. Based on (101), where do we expect θ_n to be for $n = n^*$ in (100)? Approximately at $\sqrt{2}$ rad (hence $\approx 90°$) on average, meaning almost anywhere on Ξ for a given realization.

In summary, photons emanating from a collimated beam in a scattering medium with a forward-peaked phase function have a collective memory of their original direction, but it is a relatively short term memory. The higher the number of scatterings, the more isotropic the corresponding radiance, independently of spatial considerations (boundaries, internal variability). The critical number of scatterings needed to redistribute radiance in direction space is estimated to be $\approx (1-g)^{-1}$. In a general multiple-scattering problem we can define the equivalent number of isotropic scatterings as

$$n_\mathrm{iso} = n/n^* \approx (1-g)n. \tag{102}$$

4.2 Impact of Forward Scattering on Propagation: The Transport MFP (without Fick's Law)

We are now in a position to look at the spatial consequences of the short-term memory of propagation direction due to forward-peaked but conservative ($\varpi_0 = 1$) scattering, as described in Sect. 4.1. The light particles are executing directionally-correlated random walks based on a FPD that need not be specified beyond the fact that the MFP ℓ must exist. We again assume the photons all leave the origin in direction $\mathbf{\Omega}_0$ at time $n = 0$.

(in the absence of boundary and 3D effects) is Henyey–Greenstein with $g(n) = g^n$. Since (under these same conditions) vectorial addition of random directions is determined by spherical convolutions of the PDFs that are phase functions, this implies that Henyey–Greenstein functions are the spherical equivalent of Gaussian PDFs: invariant, modulo scaling, under convolution.

[13] This 2nd-order (Gaussian) approximation is at the core of the "small-angle" approximation in RT theory used extensively in imaging and lidar studies [44].

In the discrete-time picture, the particle is then displaced from position $\boldsymbol{x}_0 = \mathbf{0}$ to $\boldsymbol{x}_1 = \boldsymbol{x}_0 + s_0\boldsymbol{\Omega}_0$, where s_0 is the initial step size. Holding $\boldsymbol{\Omega}_0$ fixed, we have

$$\mathcal{E}(\boldsymbol{x}_1) = \mathcal{E}(s_0)\boldsymbol{\Omega}_0 = \ell\boldsymbol{\Omega}_0, \tag{103}$$

using the definition of MFP in (50) or (52). From $\boldsymbol{x}_1$, and conditional to not being absorbed, the photon moves on to $\boldsymbol{x}_2 = \boldsymbol{x}_1 + s_1\boldsymbol{\Omega}_1$. It is clear that

$$\mathcal{E}(\boldsymbol{x}_2 - \boldsymbol{x}_1) = \mathcal{E}(s_1)\mathcal{E}(\boldsymbol{\Omega}_1 \bullet \boldsymbol{\Omega}_0)\boldsymbol{\Omega}_0 \tag{104}$$

since the propagation and scattering are independent, another consequence of the Markovian property of transport.

Now, after the first scattering and second step, it follows from (96) that

$$\mathcal{E}(\boldsymbol{x}_2) = [\mathcal{E}(s_0) + \mathcal{E}(s_1)\mathcal{E}(\mu_\mathrm{s})]\boldsymbol{\Omega}_0 = (1 + \varpi_0 g)\ell\boldsymbol{\Omega}_0, \tag{105}$$

where it is assumed that the 1st and 2nd FPDs have the same MFP and that an absorption may have occurred at $\boldsymbol{x}_1$ with probability $1 - \varpi_0 \geq 0$. By iteration, the independence of step-sizes and step-directions leads under the same assumption to

$$\lim_{n\to\infty} \mathcal{E}(\boldsymbol{x}_n) \bullet \boldsymbol{\Omega}_0 = \ell \sum_{n=0}^{\infty} \varpi_0^n \mathcal{E}(\mu_n) = \ell \sum_{n=0}^{\infty} (\varpi_0 g)^n = \frac{\ell}{1 - \varpi_0 g}. \tag{106}$$

So, after many scatterings, the cumulative effect of forward scattering is simply to boost the initial ballistic motion by a factor $(1 - \varpi_0 g)^{-1}$. The distance in (106) is the well-known *transport* MFP

$$\ell_\mathrm{t} = \frac{\ell}{1 - \varpi_0 g}. \tag{107}$$

Note that we have made no assumption about the FPD beyond the existence of a MFP; in particular, no spatial homogeneity assumption per se was made, only constancy of the MFP ℓ (in some spatial/ensemble average sense if required).

The emergence of the transport MFP in (107) as the residual impact of short-term directional memory on propagation is in sharp contrast with the usual derivations which come along with the diffusion/P_1 approximation to the full 3D RT problem in (1)–(3). This classic macroscopic approach to the transport problem is encapsulated in Fick's law [45], relating particle density and current:

$$\boldsymbol{F} = -\frac{c\ell_\mathrm{t}}{3} \nabla U \tag{108}$$

where

$$\left\{ \begin{array}{c} U(t, \boldsymbol{x}) \\ \boldsymbol{F}(t, \boldsymbol{x}) \end{array} \right\} = \int\limits_{4\pi} \left\{ \begin{array}{c} 1/c \\ \boldsymbol{\Omega} \end{array} \right\} I(t, \boldsymbol{x}, \boldsymbol{\Omega}) \mathrm{d}\boldsymbol{\Omega} \tag{109}$$

defines particle (in our case photon) density and current (or net vector flux), anticipating the generalization in Sect. 5.2 for time dependence.

Fick's law (108) is the *constitutive relation* that closes the macroscopic transport problem started with *continuity equation* obtained by expressing particle conservation:

$$\frac{\partial U}{\partial t} + \nabla \bullet \boldsymbol{F} + c\sigma_\mathrm{a} U = 0, \tag{110}$$

where the two last terms come from the angular integral of the steady-state 3D RT equation in (1)–(3) in the absence of sources.

At least to a first approximation, the total path L of a photon is $n \times \ell$. Notice that (for $\varpi_0 = 1$) the same answer is obtained if we reckon on the actual MFP and number of scatterings, or on the effective number of isotropic scatterings $n_{\rm iso}$ in (102) and the transport MFP $\ell_{\rm t}$ in (107). This makes physical sense since L/c is simply the time since the photon was emitted and it should not depend on whether we count actual scatterings and MFPs or effectively isotropic scatterings and transport MFPs.

In summary, photons in an isotropically scattering medium ($g = 0$) lose track of their direction of propagation at every step (average length ℓ), but it takes their positively $\mathbf{\Omega}$-correlated counterparts about $(1-g)^{-1}$ forward-peaked scatterings to "forget" their original direction.[14] In the process, this causes them to travel (on average) that much further by drifting in the original direction. So ℓ_t can be interpreted as the *effective* MFP for obtaining one isotropic scattering. Figure 7 illustrates these results in two spatial dimensions.

4.3 Asymptotics of Standard and Anomalous Diffusion in Finite Media

The overarching goal of the research program surveyed in this paper so far is to decompose ensemble-average (or large-scale) photon transport in 3D media into processes that are simpler to model, namely, diffusions. Photons diffuse in direction space and loose track of their original direction in finite time but cumulate over this time interval an extended displacement in the original direction, hence the origin of the transport MFP. To a first approximation, one can view photons executing random walks (isotropic reorientation at each step) with a mean step given by $\ell_{\rm t}$ and other aspects of the step distribution controlled by the FPD. Figure 8 illustrates schematically random walks of solar photons from the top of the atmosphere to the ground or back to space; notice how horizontal and vertical gaps in the cloudiness promote very large steps.

Adopting a Lagrangian perspective on photon transport, let $\boldsymbol{x}_0 = \mathbf{0}$ be the point of departure of the random walk:

$$\boldsymbol{x}_{n+1} = \boldsymbol{x}_n + \boldsymbol{s}, \tag{111}$$

where $\boldsymbol{s}$ is a random step drawn from the given FPD, hence

$$\boldsymbol{x}_n = \sum_{i=0}^{n} \boldsymbol{s}_i. \tag{112}$$

We are now in one of two situations. If $\mathcal{D}(s) = \mathcal{E}(\boldsymbol{s}^2) < \infty$, then

$$\mathcal{E}(\boldsymbol{x}_n^2) \sim \ell_{\rm t}^2\ n, \tag{113}$$

[14] Although it is a regime mostly of academic interest, our computations work also for $-1 \leq g < 0$. In particular, at $g = -1$ we find $\ell_{\rm t} = \ell/2$. It takes only 1/2 of a MFP (and scattering) to loose directional memory when propagation direction is exactly reversed at each event (For a given particle, all happens on a given line if $g = -1$, irrespective of dimensionality, but there is still an original direction.)

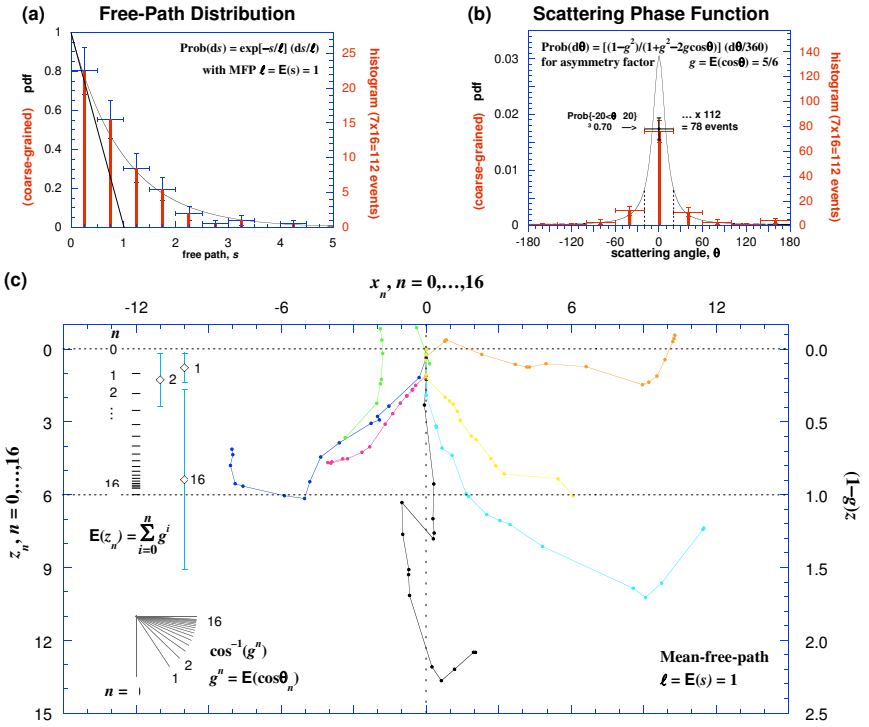

Fig. 7. Rescaling of the mean-free-path due to forward-peaked scattering in a uniform medium. **(a)** The exponential law of extinction that dictates the distribution of free paths s: $\Pr\{step \geq s\} = \exp(-s/\ell)$ with unit mean ($\ell = \mathcal{E}(s) = 1$). **(b)** The scattering kernel $p(\theta_s)$ from (33) is used, the 2D counterpart of the Henyey–Greenstein model in (30); this PDF describes the distribution of scattering angle θ_s, with an asymmetry factor $g = \mathcal{E}(\cos\theta_s) = 5/6 = 0.8333\cdots$. In panels (a-b), error bars are based on expected (Poissonian) means and variances in number of events per bin for a total of $7 \times 16 = 112$ samples. **(c)** Seven 2D particle trajectories starting straight down at the origin, all $n_{\max} = 16$ scatterings long. The l.-h. scale is in MFPs; the r.-h. z-axis uses "transport" MFPs from Eq. (107). In the lower l.-h. corner, an indication of the average direction of travel is plotted for $n = 1, \ldots, 16$ and ∞; in the upper l.-h. corner, the corresponding theoretical average positions are indicated for orders-of-scattering $n = 1, \ldots, 16, \infty$ and again for $n = 1, 2, 16$ obtained empirically, with st. dev.'s. After a number of anisotropic scatterings, the particle may just as well have been scattered isotropically once, but the MFP for such a scattering is longer by a factor $1/(1-g) = 6$. Adapted from Fig. A1 in [40]

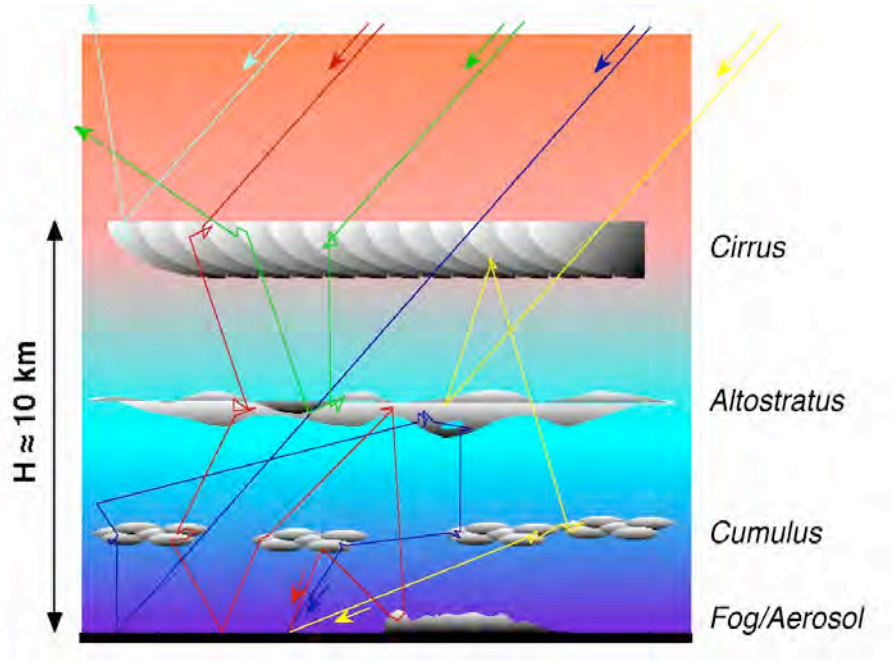

Fig. 8. Solar photons propagating in the cloudy atmosphere. We consider a wavelength where there is no absorption by cloud droplets nor gases. Each "step" in the photon's random walk is in fact rescaled, as in (107), so that the scattering can be considered isotropic. Notice how the upper (cirrus) cloud layer can let light through directly as well as produce a diffuse illumination of the lower layers; at the same time, it reflects up-welling light back towards the ground.

since we can always relate numerically the variance of the FPD to the transport MFP. However, there is another possibility ($\mathcal{D}(s) = \infty$) and another outcome:

$$\mathcal{E}(\boldsymbol{x}_n^\alpha) \sim \ell_\mathrm{t}^\alpha \; n, \tag{114}$$

where

$$\alpha = \min_q \{0 < q < 2 \; : \; \mathcal{E}(s^q) = \infty\}. \tag{115}$$

This important quantity is known as the Lévy index and it dictates the far-field behavior of the effective FPD we have adopted from (67):

$$\left\langle \left| \frac{\mathrm{d}P}{\mathrm{d}s} \right| \right\rangle \sim \frac{1}{s^{1+\alpha}}, \; s \to \infty. \tag{116}$$

We will require $\alpha > 1$ so that $\ell_\mathrm{t} = \mathcal{E}(s) < \infty$. The process described by (113) is called diffusion[15] and we will be more specific in calling it "standard" diffusion.[16] The process described by (114) is called "anomalous" diffusion.

Note that, in spite of their formal similarity, the origins of (113) and (114) are fundamentally different. The origin of (113) is the well-known law of probability that variances of sums of independent random deviates add, and we simply replaced the (finite) variance of the FPD by a dimensionally equivalent parameter (ℓ_t^2). The origin of (114) is necessarily different since $\mathcal{E}(s^\alpha) = \infty$, although it is a slow (logarithmic) divergence. So we are slightly abusing the notation $\mathcal{E}(\cdot)$ in (114) and instead interpret it as an "estimator" in sampling theory: we simply sum n random variables s taken to the power α from a PDF with property (116), and then divide by n. For a fixed n, this ratio will increase slowly as $\log n$. The sum itself, will grow as $n \log n$ times some scaling factor for the PDF which, apart from a numerical factor, can be taken as ℓ_t^α. In (114), we have summarized this argument and neglected the unimportant logarithmic term as is customary in scaling analysis.

The task now is to convert the above information above unbounded random walks in general into more useful information about random walks by photons in finite optical media. A first question we have is about the number of (effectively isotropic) scatterings $n_{\mathrm{iso},T}$ suffered by photons before crossing the medium (e.g., solar light transmitted to the ground). This is a random number of course but we can estimate approximately its mean by re-assessing (114), extended to include the case (113), as to what is given and what is averaged. If we identify the expectation (or estimation) on the l.-h. side with H^α then we can solve for a rough estimation of

$$\langle \mathcal{E}(n_{\mathrm{iso},T}) \rangle \sim (H/\ell_\mathrm{t})^\alpha. \tag{117}$$

We have yet to convert the above scale ratio into an optically meaningful quantity. Letting $\langle \tau_\mathrm{c} \rangle$ denote the ensemble-average cloud optical thickness, we have

$$H/\ell_\mathrm{t} \mapsto (1-g)\langle\sigma\rangle H = (1-g)\langle\tau_\mathrm{c}\rangle \tag{118}$$

at non-absorbing wavelengths, i.e., when ϖ_0 in (12) is unity.

As it turns out, $\mathcal{E}(n_{\mathrm{iso},T})$ and even $\mathcal{E}(n_T)$ are not readily observable quantities while the transit time (a continuous random variable) is.[17] A more convenient assessment of transit time is therefore total photon path length L_T which is roughly

[15] This nomenclature is fully consistent with the diffusion approximation obtained in a variety of ways from the traditional Eulerian perspective used in transport theory.

[16] For the classic Eulerian derivation of (113), we substitute (108) into (110) with $\sigma_\mathrm{a} = 0$. This yields the prototypical parabolic PDE $\partial_t U = D\nabla^2 U$, where $D = c\ell_\mathrm{t}/3$ is the diffusivity (assumed constant), to which we apply the initial condition $U(\boldsymbol{r}, 0) = \delta(\boldsymbol{r})$. The well-known solution for $t > 0$ is $U(\boldsymbol{r}, t) = \exp(-\boldsymbol{r}^2/4Dt)/(4\pi Dt)^{3/2}$. Recall now that, with this normalization, density U is simply the probability of finding the diffusing particle at position $\boldsymbol{r}$ at time t. Thus $\mathcal{E}(\boldsymbol{r}^2|t) = \int_0^\infty \boldsymbol{r}^2 U(\boldsymbol{r}, t)\mathrm{d}\boldsymbol{r} = Dt$ where we can identify the continuous time t with pathlength $\ell_\mathrm{t} n$ in (113) divided by c.

[17] For transit time, we can use either a pulsed laser or the absorption by a uniform gas (cf. Sect. 5) while for estimating order of scattering statistics we would need to use an absorption feature of the scattering particles, here, the cloud water droplets.

ℓ (ℓ_t) times n_T ($n_{\mathrm{iso},T}$). For means, we have

$$\mathcal{E}(L_T) \approx \ell\mathcal{E}(n_T) \approx \ell_\mathrm{t}\mathcal{E}(n_{\mathrm{iso},T}). \tag{119}$$

Assembling the information in the last three equations, we find

$$\langle\mathcal{E}(L_T)\rangle \sim [(1-g)\langle\tau_\mathrm{c}\rangle]^{\alpha-1}H. \tag{120}$$

Another observable and radiometrically important quantity is the probability T of photon transmission through the medium, irrespective of the transit time. To access this deceptively simple property, we need to invoke a lesser-known law for random walks on a half-space. If the random walking particles all leave the plane $z = 0$, how many steps does it take to return to the plane of departure? It is easy to see the analogy with photon reflection from a semi-infinite optical medium, and the answer is [46, 47]

$$\Pr\{\text{(discrete) return time} \geq n\} \sim 1/\sqrt{n} \tag{121}$$

in the regime $n \gg 1$. This remarkable PDF has infinite variance and infinite mean (only moments of order $<1/2$ converge). Davis and Marshak [40] brought together the straightforward estimation of $\langle\mathcal{E}(n_{\mathrm{iso,T}})\rangle$ in (121) and (117) to estimate transmission probability

$$\Pr\{\text{return time} \geq \langle\mathcal{E}(n_{\mathrm{iso},T})\rangle\} \sim \ (H/\ell_\mathrm{t})^{-\alpha/2}. \tag{122}$$

In more optical terms, we have

$$T \sim [(1-g)\langle\tau_\mathrm{c}\rangle]^{-\alpha/2}. \tag{123}$$

With so many layers of approximation, it is hard to take the generalized (standard and anomalous) photon diffusion theory we have just exposed seriously as a model of radiation transport in the Earth's cloudy atmosphere. However, the theory does make specific predictions for observable quantities in the time-domain (120) and in steady-state (123). In the next section, we show using both new simulations and new observations that the phenomenology of generalized photon diffusion does seem to capture key aspects of real 3D RT in the real atmosphere.

5 Large-Scale 3D RT Effects in Cloudy Atmospheres

5.1 Overcoming the Challenge of Observing 3D Effects in Steady-State RT

The theoretical result in (123) is clear, and it has been the same message from any other domain-average model [48]: 3D variability (here, measured by $2-\alpha > 0$) systematically enhances photon transmission through the atmosphere to the ground. It is not however straightforward to demonstrate observationally that 3D RT effects have an impact on very large domains. Indeed, it is easy to obtain large-scale radiances from satellites (they are essentially the raw data), but fluxes are elusive (they call for angular conversion models). Furthermore, it is non-trivial to estimate

what the domain-average optical depth is and that is necessary to make an independent prediction based on 1D RT. When using satellites with large-enough pixels, we tend to use said 1D RT models in inversion mode, which of course only gives us the "effective" optical depth that is needed to drive the 1D RT model to give us the observed radiance or flux.[18] It is then tempting to compare this estimate of τ_c with independent ground-based and in-situ estimates, and many studies have done that. However, the space-time sampling volumes of surface and airborne sensors is radically different from their space-borne counterparts. Then we can try to convince ourselves that the obvious 3D RT effects (shadows, over-illumination, etc.) are small-scale and of varying sign. So, upon large-scale —and moreover angular— averaging, they will surely all but vanish. Not so!

In recent years, increasing sophistication in multi-spectral, multi-angle and/or multi-resolution methods have shed new light on this difficult problem in cloud remote sensing [38]. Interestingly, the most compelling direct observational evidence for the impact of 3D cloud structure on large-scale atmospheric radiation processes comes from time-domain RT [49]. This is not very surprising for the physics and engineering communities which have been forever using "impulse responses" to probe systems with complex, possibly unknown, internal structure. The α-dependence in the asymptotic ensemble-average 3D RT result in (120) for pathlengths of transmitted photons gives us a hint. The real surprise is however that this time-dependent 3D RT can be performed observationally using abundant and free solar photons rather than power-hungry pulsed lasers.

5.2 Time-Dependent 3D RT ... with Solar Photons

Let us now open up the deterministic 3D RT problem described in (1)–(3) to time dependence: $I(\boldsymbol{x}, \boldsymbol{\Omega}) \mapsto I(t, \boldsymbol{x}, \boldsymbol{\Omega})$. The advection operator is changed accordingly:

$$\mathcal{L} = \boldsymbol{\Omega} \bullet \nabla + \sigma(\boldsymbol{x}) \mapsto \frac{1}{c}\left(\frac{\partial}{\partial t}\right) + \boldsymbol{\Omega} \bullet \nabla + \sigma(\boldsymbol{x}). \tag{124}$$

Without loss of generality (because of the superposition principle), we can consider the source term as delta-in-time: $Q(\boldsymbol{x}, \boldsymbol{\Omega}) \mapsto Q(t, \boldsymbol{x}, \boldsymbol{\Omega}) = q(\boldsymbol{x}, \boldsymbol{\Omega})\delta(t)$. We note that even in steady-state RT sources and radiances all have raw units of "per second" because, after all, this is transport theory and particles take time to move. Here we have a finite number of particles $\int\int q(\boldsymbol{x}, \boldsymbol{\Omega})\,\mathrm{d}\boldsymbol{x}\mathrm{d}\boldsymbol{\Omega}$ that are released all at once and we monitor how they spread in time, until they are absorbed or have escaped ("absorbed" by a boundary).

A deep beauty of general time-dependent transport theory is that this is not really a new class of problems [50, 51]. Indeed, first we make the convenient change of variables in (and of units for) I and Q: $I(t, \cdots) \mapsto I(L, \cdots)$ where pathlength $L = ct$, and similarly for Q. Now we take the Laplace transform of I with respect to path L:

$$\tilde{I}(k, \cdots) = \int_0^\infty \mathrm{e}^{-kL} I(L, \cdots)\mathrm{d}L, \tag{125}$$

[18] Circularity notwithstanding, this effective τ_c is all that is required anyway in many climate-driven applications.

where k is at present just the Laplace conjugate of path L (in units of m^{-1}). We also Laplace transform the time/path-dependent 3D RT equation: for the advection operator in (124),

$$\tilde{\mathcal{L}} = \boldsymbol{\Omega} \bullet \nabla + \sigma(\boldsymbol{x}) + k, \tag{126}$$

while $\tilde{Q}(k, \boldsymbol{x}, \boldsymbol{\Omega}) = q(\boldsymbol{x}, \boldsymbol{\Omega})$. So $\tilde{I}$ simply obeys a steady-state 3D RT equation with an enhanced extinction term. Not any kind of enhancement. Specifically, because the scattering process in (3) in unaffected, it is the absorption coefficient $\sigma_\mathrm{a}(\boldsymbol{x})$ in (13) that is *uniformly* boosted by an amount k. Physically, this amounts to adding to the structured 3D scattering/absorbing medium a uniform gas that only absorbs photons at a rate of k per unit of length along any beam. This formal mapping of the temporal Green function problem in 3D RT to a steady-state 3D RT problem with (more) gaseous absorption —and sometimes simply (125) with the notation $I(L, \cdots) = \tilde{I}(0, \cdots) \times p(L, \cdots)$ for the pathlength PDF— is called the "equivalence theorem."

Now suppose we are interested in computing the moments $\mathcal{E}(L^n)$, $n = 1, 2, 3, \ldots$, at some position $(\boldsymbol{x}, \boldsymbol{\Omega})$ in photon phase-space. By definition, we have

$$\mathcal{E}(L^n | \cdots) = \int_0^\infty L^n I(L, \cdots) \mathrm{d}L \; / \int_0^\infty I(L, \cdots) \mathrm{d}L. \tag{127}$$

From (125), we can obtain these integrals by successive orders of differentiation in the Laplace-transformed quantities:

$$\mathcal{E}(L^n | \cdots) = \frac{1}{\tilde{I}(0, \cdots)} \left(-\frac{\mathrm{d}}{\mathrm{d}k} \right)^n \tilde{I}(k, \cdots) \Big|_{k=0}. \tag{128}$$

We assume, just for simplicity at present, that the *only* absorption is by the well-mixed (uniform) gas characterized by k. Then, in principle, one can derive the statistical moments of pathlength from the behavior of steady-state radiance, denoted here by $\tilde{I}(k, \cdots)$, in weak-absorption limit ($k \to 0$). Finally, we note that (128) carries over to any integration over the position $\boldsymbol{x}$ or angular $\boldsymbol{\Omega}$ variables.

5.3 Some Recent Observations

We are extremely fortunate in atmospheric science that the above program can be implemented thanks to the sharp spectral features of molecular oxygen that occur near the peak (in photon number) of the solar spectrum. The spectro-radiometric technology required for robust pathlength moment estimation has been maturing over the past 15 or so years and so has the analysis methodology, which is not quite as simple as in (128) because of finite spectral resolution effects, cf. Min and Harrison [52, 53]. Even though the phenomenology of anomalous photon diffusion from Sect. 4.3 is not well known, there is a growing awareness that pathlength statistics convey information about the spatial variability of clouds, cf. recent review article by Stephens et al. [49]. Several groups have investigated mean photon pathlength in transmission (i.e., using ground-based instruments), mostly in conjunction with optical depth, with [14, 54] or without [55, 56] reference to the anomalous diffusion/Lévy walk model. We now examine some recently published observations and analyses.

Figure 9 is a composite of figures from the recent paper by Scholl et al. [15]. It shows O_2-based photon pathlength observations and ancillary cloud diagnostics; I refer the reader to the original paper for all instrumental and data analysis details. In the upper panel we see an evolving cloud episode using a sophisticated mm-radar profiler [57]. Over the hour-long observation period (extracted from a much longer one), two well-defined cloud layers become gradually thinner, more tenuous, and more disjoint. The upper layer between 9 and 10 km in altitude is a cirrus (ice-crystal) cloud. Cirrus layers are typically highly textured (think "angel-hair" clouds) and generally semi-opaque in the sense that sunlight cannot get directly through but, thanks to the strongly forward-scattering phase function, one can still see the location of the bright solar source; at the same time, cirrus layers are powerful diffusers of sunlight. The lower cloud deck, below 2 to 1 km, starts as a dense boundary-layer cloud, probably a strato-cumulus, that are invariably made of liquid water droplets. It is clearly producing in-cloud drizzle and maybe even ground-level rain between 12:14 and 12:22 Z; after that episode, it rapidly breaks up.

In the middle panel we see the mean pathlength $\mathcal{E}(L_T)$ of transmitted solar photons (in units of cloud-system thickness H) plotted versus rescaled optical depth $(1-g)\tau_c$; the pathlength statistics were derived from a high-resolution spectro-radiometer fed by fore-optics with narrow field-of-view (0.86°) centered on the zenith. The theoretical curves are inspired by the power-law relation predicted in (120). Specifically, a more detailed diffusion-theoretical formula for $\mathcal{E}(L_T)/H$ by Davis and Marshak [58], valid only in the standard $\alpha = 2$ case but including pre-asymptotic corrections, is

$$\mathcal{E}(L_T)/H = \frac{1}{2} \times (1-g)\tau_c \times \left[1 + \frac{\epsilon}{2}\left(\frac{4+3\epsilon}{1+\epsilon}\right)\right] \tag{129}$$

where[19]

$$\epsilon = 2\chi/(1-g)\tau_c \tag{130}$$

becomes small as τ_c increases without bound. Scholl et al. simply took the right-hand side of the above expression for $\mathcal{E}(L_T)/H$ to the power $(\alpha - 1)$. This ansatz gives the correct asymptotic behavior in (120) and also a physically reasonable value of $3\chi/2$, which is numerically equal to or slightly larger than unity, for $\tau_c \to 0$ (even though diffusion is not a good model for transport in that limit of thin media) and $\alpha \to 1$. As expected, we see the observed data pointing towards α-values for the most part significantly less than 2. Also, the *effective* α value thus retrieved from the data decreases as expected when the clouds break up.

The lower panel shows the ratio $\sqrt{\mathcal{E}(L_T^2)}/\mathcal{E}(L_T)$ versus $(1-g)\tau_c$. We see that this RMS-to-mean ratio for transmitted photon pathlengths is only weakly dependent on optical thickness. This is as predicted by Davis and Marshak [58] in the $\alpha = 2$ case, cf. solid curve which is based on (129) and a like expression for the RMS pathlength (only with a different prefactor and correction term). According to the observations, this weak dependence seems to generalize to situations where $\alpha < 2$. The 2nd-order

[19] In the diffusion approximation, parameter χ in (130) arises in the (mixed) boundary conditions applied to the parabolic PDE that determines photon density U inside a uniform slab. This PDE results from combining (110) with (108) and $\chi\ell_t$ is the so-called "extrapolation length" [45]. Values of $\chi = 2/3$ or $\chi = 0.71$ have been used, depending on the quantity of interest and the required accuracy [58].

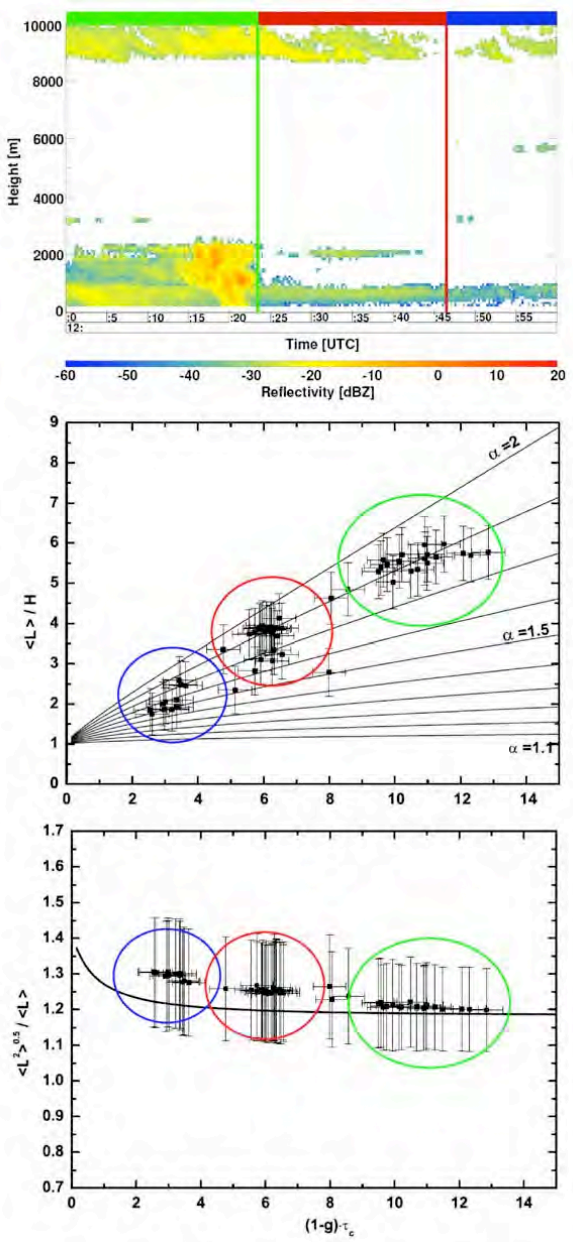

Fig. 9. Solar photon pathlengths and coincident cloud structure at Cabauw (the Nederlands) on May 22, 2003, between 12:00 and 13:00 Z. **(upper)** Time-series of reflectivity profiles from the up-looking KNMI 35 GHz radar [57] which is sensitive to cloud droplets; three distinct periods are defined (color-coded) as the two well-defined cloud layers thin and break up. **(middle)** Mean pathlength cumulated inside the cloudy region (base of lowest cloud to top of highest) versus rescaled cloud optical depth $(1-g)\tau_c$: observations with their uncertainties and theoretical predictions parameterized by α, as explained in the text. **(lower)** RMS-to-mean ratio for pathlength versus $(1-g)\tau_c$: observations with their uncertainties and a theoretical prediction for the $\alpha = 2$ case, as explained in the text. (Adapted from Figs. 11–13 in [15], with permission)

moment of transmitted solar photons was previously investigated observationally by Min et al. [54], also thanks to enhanced instrumental capability. When comparing pathlength mean and variance, these authors found compatibility with the Davis and Marshak predictions for the $\alpha = 2$ case but rather as an extreme situation. However, their data was normalized and plotted differently than in the lower panel of Fig. 9; so there does not seem to be any contradiction.

In the following, I describe a new 1D transport theory with a power-law propagation kernel that accounts for all the observed properties of transmitted solar photons.

5.4 A New 1D Theory

From the outset of this paper, we have used the standard Eulerian framework of RT based on the 3D linear transport equation and describing all the dependent and independent variables, the relevant coefficients, the BCs, and so on. We then drifted towards an ever more Lagrangian outlook, describing in detail —at times graphically— how individual photon beams interact with homogeneous and variable optical media: propagation, scattering, and so on. We now return to an Eulerian perspective on RT in order to formulate a more general class of 1D models inspired by our findings on the systematic effects of 3D spatial variability on the propagation process. This new model will of course neatly explain the new observations described in the previous subsection.

First, we review standard 1D RT modeling when the sources are azimuthally symmetric (equivalently, azimuthally-averaged). We thus wish to determine the radiance function $I(z, \mu)$ of two variables $0 < z < H$ and $-1 \leq \mu \leq +1$ that obeys

$$\mu \frac{\mathrm{d}I}{\mathrm{d}z} = \sigma \left[-I(z,\mu) + \frac{\varpi_0}{2} \int_{-1}^{+1} \mathring{p}(\mu', \mu) I(z, \mu') \mathrm{d}\mu' \right], \tag{131}$$

with the following very specific BCs

$$\begin{cases} I(0,\mu) = F_0/\pi, & 0 < \mu \leq +1 \quad \text{(diffuse irradiance)} \\ I(H,\mu) = 0, & -1 \leq \mu < 0 \quad \text{(vacuum)} \end{cases} \tag{132}$$

where F_0 is the incoming flux. Immediate inspection of the above problem tells us that the usual change of variables, from physical to optical depth,

$$\begin{cases} \mathrm{d}z \mapsto \mathrm{d}\tau = \sigma \mathrm{d}z, \text{ and} \\ H \mapsto \tau_\mathrm{c} = \sigma H \text{ in the BCs,} \end{cases} \tag{133}$$

is in order.[20] This amounts to using the (constant) MFP $\ell = 1/\sigma$ as the unit of length and it is indeed one of the fundamental length scales of the problem, the other being cloud thickness H.

In (131), we use the azimuthally-averaged phase function

$$\mathring{p}(\mu', \mu) = \frac{1}{2\pi} \int_0^{2\pi} p(\mu\mu' + \sqrt{1-\mu^2}\sqrt{1-\mu'^2}\cos\phi) \mathrm{d}\phi. \tag{134}$$

[20] This is useful even if extinction σ and other parameters, ϖ_0 and $\mathring{p}(\mu', \mu)$, were to depend on z.

If discrete ordinates are used, there is no need to Fourier decompose the problem into as many decoupled 1D RT equations; only the discrete values of $\mathring{p}(\mu',\mu)$ are required. By reciprocity, we of course have $\mathring{p}(\mu,\mu') = \mathring{p}(\mu',\mu)$. If spherical harmonics are used, then one must invoke [59]

$$\mathring{p}(\mu',\mu) = \frac{1}{4\pi}\sum_{n\geq 0}(2n+1)\eta_n P_n(\mu)P_n(\mu'). \tag{135}$$

In the case of the Henyey–Greenstein phase function, we recall from (31) that $\eta_n = g^n$.

To formulate the integro-differential problem in (131)–(132), we can also use the integral form $I = \mathcal{K}_\infty I + I_0$ from (4) where

$$\mathcal{K}_\infty(\sigma H,\varpi_0,g)[\cdot] = \sigma\frac{\varpi_0}{2}\left\{\begin{array}{ll}\int_z^H \mathrm{d}z'\int_{-1}^{+1}\mathring{p}_g(\mu',\mu)\mathrm{e}^{-\sigma(z'-z)/|\mu'|}[\cdot]\mathrm{d}\mu'/|\mu'|, & \mu>0\\ \int_0^z \mathrm{d}z'\int_{-1}^{+1}\mathring{p}_g(\mu',\mu)\mathrm{e}^{-\sigma(z-z')/|\mu'|}[\cdot]\mathrm{d}\mu'/|\mu'|, & \mu<0\end{array}\right. . \tag{136}$$

In the arguments of the kernel $\mathcal{K}_\infty$ we have anticipated the usual change of variables, from physical to optical units of depth, in (133). The BCs in (132) dictate the forcing term,

$$I_0(z,\mu) = \frac{F_0}{\pi}\exp(-\sigma z/\mu), \tag{137}$$

corresponding to diffuse irradiation at the cloud top ($z = 0$) and an absorbing lower boundary ($z = H$). As recalled in the Introduction, this problem is formally or computationally solved by iteration. But why the subscript "∞"?

The exponential terms in the transport kernel (136) and the uncollided flux (137) have very specific physical meanings: we are looking respectively at the FPD (grouping the exponential with the σ) and the probability of transmission from the boundary to a distance $s = z/\mu$ where the first scattering (or absorption) happens. We propose simply to replace these as follows. First, the direct transmission term $\exp(-\sigma z/\mu)$ in (137) becomes

$$\langle P(s)\rangle = \langle T_{\mathrm{dir}}\rangle(s;\langle\sigma\rangle,a) = \frac{1}{(1+\langle\sigma\rangle s/a)^a} \tag{138}$$

from (87) with $s = z/\mu$. Second, the FPD term $\sigma\exp(-\sigma|z'-z|/|\mu'|)$ in (136) becomes

$$\langle p(s)\rangle = \left|\left(\frac{\mathrm{d}}{\mathrm{d}s}\right)\langle T_{\mathrm{dir}}\rangle\right|(s;\langle\sigma\rangle,a) = \frac{\langle\sigma\rangle}{(1+\langle\sigma\rangle s/a)^{a+1}} \tag{139}$$

with $s = |z'-z|/|\mu'|$.

This leads to the more general class of 1D integral transport equation to solve based on the kernel

$$\mathcal{K}_a(\langle\sigma\rangle H,\varpi_0,g)[\,\cdot\,] = \langle\sigma\rangle\frac{\varpi_0}{2}\times$$
$$\left\{\begin{array}{ll}\int_z^H \mathrm{d}z'\int_{-1}^{+1}\mathring{p}_g(\mu',\mu)\left(1+\frac{\langle\sigma\rangle(z'-z)}{a|\mu'|}\right)^{-(a+1)}[\cdot]\mathrm{d}\mu'/|\mu'|, & \mu>0\\ \int_0^z \mathrm{d}z'\int_{-1}^{+1}\mathring{p}_g(\mu',\mu)\left(1+\frac{\langle\sigma\rangle(z-z')}{a|\mu'|}\right)^{-(a+1)}[\cdot]\mathrm{d}\mu'/|\mu'|, & \mu<0\end{array}\right. , \tag{140}$$

where $a > 0$. The choice of arguments again reflects that we can make the natural change of spatial variable in (133): $\mathrm{d}z \mapsto \mathrm{d}\langle\tau\rangle = \langle\sigma\rangle\mathrm{d}z$ and $H \mapsto \langle\tau_{\mathrm{c}}\rangle = \langle\sigma\rangle H$.

However, $\langle\tau\rangle$ can no longer be interpreted as the physical depth z measured in units of MFP because the MFP is no longer $1/\langle\sigma\rangle$ and is indeed systematically longer, cf. (88). The uncollided radiance term is also changed, in this case, to

$$I_0(z,\mu) = \frac{F_0}{\pi}\left(1+\frac{\langle\sigma\rangle z}{a|\mu|}\right)^{-a}, \tag{141}$$

with $a > 0$. As previously shown, all these expressions give the proper limits for $a \to \infty$ as long as we identify the *mean* extinction $\langle\sigma\rangle$ with the uniform (a.k.a. in probability as the "degenerate") value σ.

What results are we particularly interested in? The total transmission is one of them, namely,

$$T_a(\langle\tau_c\rangle, \varpi_0, g) = \frac{2\pi}{F_0}\int_0^1 \mu I(H,\mu)\mathrm{d}\mu \tag{142}$$

as it measures the mean particle current through the medium. In atmospheric RT, this is the amount of spectral radiation that reaches a dark surface, such as the ocean. To compute the radiant energy sent immediately back to space, as well as total flux reaching a partially reflective surface, we need the albedo

$$R_a(\langle\tau_c\rangle, \varpi_0, g) = \frac{2\pi}{F_0}\int_{-1}^0 |\mu| I(0,\mu)\mathrm{d}\mu, \tag{143}$$

In remote sensing applications, we are limited to sampling radiance in direction space rather than obtaining the above integrals. So we shall turn our modeling interests towards "zenith" radiance at ground level (here, $z = H$) and "nadir" radiance at the top-of-the-atmosphere (here, $z = 0$): respectively,

$$I_a^{\downarrow}(\langle\tau_c\rangle, \varpi_0, g) = \frac{\pi I(H,+1)}{F_0} \tag{144}$$

and

$$I_a^{\uparrow}(\langle\tau_c\rangle, \varpi_0, g) = \frac{\pi I(0,-1)}{F_0}, \tag{145}$$

where we have opted for so-called "Bidirectional Reflection Function" units.[21]

If, beyond the above steady-state quantities (for any $\varpi_0 \leq 1$), we are interested in statistics of pathlength L (usually for the conservative case $\varpi_0 = 1$) then we can apply the corollary of the equivalence theorem in (128) using the simple change of variables $\varpi_0 \mapsto k = (1-\varpi_0)\langle\sigma\rangle$, hence

$$\varpi_0 = 1 - kH/\langle\tau_c\rangle. \tag{146}$$

This means that the expression in (128) for the nth-order pathlength moments ($n = 1, 2, 3, \ldots$) now reads as

[21] In these convenient "BRF" units, there is no difference in numerical values between albedo —or transmittance in the case of (144)— and radiance if it is isotropic (a.k.a. Lambertian). If not, which is of course the generic case, then we can interpret the radiance as an effective albedo or transmittance for the particular direction of interest.

$$\mathcal{E}(L^n|\cdots)/H^n = \langle\tau_c\rangle^{-n}\left[\frac{1}{I(\cdots)}\left(-\frac{\partial}{\partial\varpi_0}\right)^q I(\cdots)\right]_{\varpi_0=1} \tag{147}$$

where we have normalized the pathlengths by H and let $(\cdots)$ represent both photon phase-state variables (z,μ) *and* parameters of the optical medium $(\langle\tau_c\rangle,\varpi_0,g)$. We have also dropped the tildes and the explicit dependence on $k(\varpi_0)$ in (128) since it is now just a parameter of the 1D RT problem.

Recall that the recipe in (147) can be applied to any of the above angularly integrated or sampled quantities, namely, $I(\cdots)\mapsto T_a(\cdot)$ or $I_a^{\downarrow}(\cdot)$ at $z=H$ or else $R_a(\cdot)$ or $I_a^{\uparrow}(\cdot)$ at $z=0$ where $(\cdot)$ now represents only optical parameters. After using (147), the H-normalized pathlength moments for boundary fluxes or z-axis radiances will depend only on $\langle\tau_c\rangle$ and g. The Lagrangian asymptotic analysis of the previous section suggests this dependence should collapse onto a power-law in $(1-g)\langle\tau_c\rangle$ for large enough values. But what is the connection between $a>0$ and $\alpha<2$ from Sect. 4.3? Recalling that α is the critical (logarithmically divergent) moment of the FPD, we see that

$$\alpha = \min\{a,2\}, \tag{148}$$

irrespective of the phase function's properties (i.e., g) which can only impact low orders of scattering.

The remaining and important question is how do we numerically solve the problem in (4) with (140) and (141)? It will be interesting to see how discrete ordinates and spherical harmonics apply to the new class of 1D transport problems in (140)–(141). What is clear at present is that there is an intimate connection between the exponentials in (136)–(137) and the 1D differential equation formulation in (131) —and this differential formalism plays a key role in obtaining some of the classic numerical solutions [60]. There is no integro-differential equivalent of (140)–(141) where power-law kernels appear. Expressions with pseudo-differential operators[22] may exist, but this remains an open question. See Buldyrev et al. [61] for a positive answer to this question for a related (strictly Lévy) type of propagation kernel.

If one is only interested in the boundary fluxes (142)–(143), then the easiest is certainly to use a basic Monte Carlo algorithm. Bearing in mind the general theory of the method, all we need to do as far as the random particle trajectory is concerned is to replace the single line of code that executes (48) by

$$s = (\xi^{-1/a}-1)\times\frac{a}{\langle\sigma\rangle}, \tag{149}$$

where, if H and $\langle\tau_c\rangle$ are the given quantities, we use $\langle\sigma\rangle=\langle\tau_c\rangle/H$. If one is only interested in the outgoing radiances (144)–(145) then Monte Carlo is still the easiest way to go although we will also need the probability of direct transmission to the upper or lower boundary according to (138), with $s=z$ and $H-z$ respectively, to compute weights in the local estimation technique [62]. Last but not least, the Monte Carlo method enables direct estimation of the normalized moments in (147) while tracing the particle trajectories under the assumption that $\varpi_0=1$.

Figure 10 shows numerical results for lower-boundary (i.e., transmission) quantities for five incarnations of the 1D transport model: the standard case ($a=\infty$),

[22] A good example is $(-\nabla^2)^\gamma$, for $0<\gamma<1$ which can be implemented easily in Fourier space in the form of a high-pass filter in $k^{2\gamma}$.

and 4 new cases ($a = 1.2, 1.4, 1.6, 1.8$) where the MFP is still finite. In all cases, the scattering kernel $p(\mathbf{\Omega}' \bullet \mathbf{\Omega})$ was Henyey–Greenstein with $g = 0.85$. Panel (a) shows $T_a(\langle\tau_c\rangle, 1, g)$ versus $(1-g)\langle\tau_c\rangle$ in log-log axes; we see that the anomalous asymptotic scaling in (123) is indeed realized with α from (148) at large enough $\langle\tau_c\rangle$. The same remark applies to $I_a^{\downarrow}(\langle\tau_c\rangle, 1, g)$ in panel (b) that furthermore shows the characteristic linear increase with optical depth at small values. A maximum in $I_a^{\downarrow}(\langle\tau_c\rangle, 1, g)$ is reached between $(1-g)\langle\tau_c\rangle \approx 1/3$ ($a = \infty$) and ≈ 1 ($1 < a < 2$). Panels (c) and (d) display in lin-lin axes respectively the mean and RMS-to-mean ratio for pathlengths based on $I_a^{\downarrow}$ in (147).

Where the asymptotic regime starts can be determined visually by examining Figs. 10a–b: we see that the scaling predicted for $T_a(\langle\tau_c\rangle, 1, g)$ in (123) seems to begin at $(1-g)\langle\tau_c\rangle \approx 10$ (i.e., $\langle\tau_c\rangle \approx 70$ for $g = 0.85$) for the selected values of $a = \alpha$ between 1.2 and 1.8; this threshold is practically off the chart in Fig. 10c (which was designed to have the same span as the middle panel of Fig. 9). It is well-known — and we clearly see— that asymptotic behavior starts much sooner for the standard exponential kernel ($a = \infty$), near $(1-g)\langle\tau_c\rangle \approx 2$ (i.e., $\langle\tau_c\rangle \approx 13$ for $g = 0.85$). We understand the delayed transition to asymptotic scaling in transmission and in mean pathlength when a decreases from ∞ to unity as a consequence of the growth of the optical (physical) thicknesses of the top and bottom boundary layers for fixed $\langle\tau_c\rangle$ (H and $\langle\sigma\rangle$). Indeed, according to (88) and (106), the relevant transport MFP is

$$\ell_t(a) = \frac{\langle\mathcal{E}(s)\rangle}{1-\varpi_0 g} = \frac{a}{a-1} \times \frac{H}{(1-\varpi_0 g)\langle\tau_c\rangle}, \tag{150}$$

a natural estimate for the boundary layer thickness, that increases without bound as $a \to 1$. As a gets close to unity, the two boundary layers have invaded the whole domain; physically, the presence of the boundaries can be felt at all levels in the medium because of the long tail of the propagation kernel in (139). If we retain the often quoted criterion [63], from the $a = \infty$ case, for the onset of asymptotic behavior,

$$2 \times \frac{\ell_t(\infty)}{H} = \frac{2}{(1-\varpi_0 g)\langle\tau_c\rangle} \lesssim 1, \tag{151}$$

then here we have:

$$(1-\varpi_0 g)\langle\tau_c\rangle \gtrsim \frac{2a}{a-1} \tag{152}$$

which ranges from 4 to 12 for $1.2 \leq a \leq 1.8$, more-or-less as observed in the numerical simulations.

On purpose, Fig. 10c for $\mathcal{E}(L)/H$ versus $(1-g)\langle\tau_c\rangle$ mimics the display of observations in the middle panel of Fig. 9. We see that, although they are not plotted, the data points populate a region where we will find transport models with $2 < a < \infty$. Such models have the same asymptotic scaling as the $\alpha = 2$ case, but its onset as optical depth increases is delayed beyond an already quite large value estimated by Davis and Marshak [58] to be $\approx$10 for $(1-g)\tau_c$. Consequently, it is now clear that

1. the observations of Scholl et al. are mostly *not* in the asymptotic transport regime, and
2. a model such as the present 1D integral transport equation that accounts for pre-asymptotic behavior is required to further exploit atmospheric A-band data.

Our final Fig. 10d shows the same RMS-to-mean ratio as in the lower panel of Fig. 9 on the same vertical and horizontal scales. We see that the new model explains

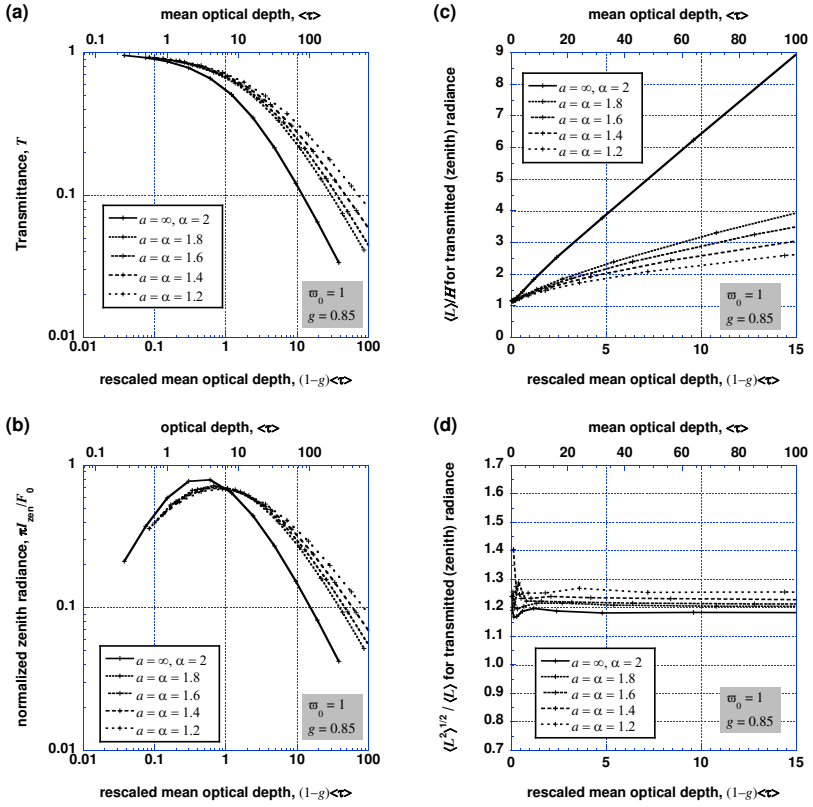

Fig. 10. Results from Monte Carlo solutions of the new 1D integral transport equation in (4) using (140)–(141) with $\varpi_0 = 1$ and $g = 0.85$. **(a)** Log-log plot of transmission in (142) as a function of $(1-g)\langle\tau_c\rangle$ for $a = 1.2, 1.4, 1.6, 1.8$, and ∞. **(b)** Same as (a) but for zenith radiance in (144). In both panels, we see the predicted scaling in $\langle\tau_c\rangle^{-\alpha/2}$ for large enough values. **(c)** Lin-lin plot of $\mathcal{E}(L)/H$ from (147) with $n = 1$ using $I_a^{\downarrow}$ where we see the predicted scaling in $\langle\tau_c\rangle^{\alpha-1}$ for large values; by comparison with the middle panel of Fig. 9, we also note that the observations point to a-values between 2 and some relatively large value rather than α-values per se smaller than 2. **(d)** Same as (c) but for $\sqrt{\mathcal{E}(L^2)}/\mathcal{E}(L)$ where we confirm the recent observation that the RMS path scales like the mean independently of a or α, cf. Fig. 9.

Numerical Details: The MFP $\langle\ell\rangle = a/(a-1)\langle\sigma\rangle$ was set to unity and 11 physical thicknesses were examined: $H = 2^{-2,\ldots,8}$. This was done in a single run for a given value of a, by flagging the history as to which of the 11 media it had not yet escaped. The mean optical thickness $\langle\tau_c\rangle = \langle\sigma\rangle H$ was computed after the fact from a and H. For each run, 5×10^6 histories were generated. This resulted in a maximum of 23249, 26317, 24997, 31306, and 44953 scatterings respectively for $a = 1.2, 1.4, 1.6, 1.8$, and ∞ in the case where $H = 256 \times \langle\ell\rangle$.

well the weak dependence on optical depth with furthermore the right trends in both a and $\langle \tau_c \rangle$. However, we must emphasize here that the choice of upper BC in (132) that expresses diffuse isotropic illumination (equivalently, the source terms (137) and (141)) is important to obtain the observed trend at small optical depths. This makes physical sense because the upper level of "cloud" is, by definition, a strong diffuser.[23]

This last finding sheds new light on the phenomenology of particle transport with power-law FPDs presented in Sect. 4.3. That approach was entirely predicated on a judicious truncation of the universal law that describes the distribution along orders-of-scattering of particles reflected from a semi-infinite isotropically scattering medium. The tight connection we found numerically between $\sqrt{\mathcal{E}(L^2)}$ and $\mathcal{E}(L)$ tells is that this truncation has to be a very sharp one indeed, irrespective of the finite optical thickness of the medium. Otherwise, significant numbers of straggling particles would affect the higher-order moments.

6 Concluding Remarks

We have investigated the impact of unresolved spatial variability on linear particle transport systems at the most fundamental level (i.e., incoherent geometric optics in the case of our primary application to atmospheric radiative transfer). The elementary process of interest here is propagation between an emission or scattering event and the next scattering event or an absorption/escape. In uniform regions —a tempting *assumption* to make when structure is unknown— this propagation is controlled by an exponential decay in particle flux along a given beam (the well-known Beer's law in radiative transfer). Concurring with other authors, I showed that *on average* this decay is in fact sub-exponential in random but spatially correlated media. This is established using both transport-theoretical methods and a somewhat deeper point-process approach pioneered by A. Kostinski and coworkers. Furthermore, the *actual* mean-free-path is systematically larger than predicted with a uniform-medium assumption based on mass conservation. Finally, for the predicted extension of the mean-free-path and systematic deviation from exponential decay to matter, there needs to be spatial correlations at scales commensurate with the (actual) mean-free-path.

Two important consequences are:

- Generally speaking, homogenization (or "effective medium") theory can capture the extended mean-free-path effect but, being limited to exponential kernels, it will fail to capture other effects at scales much larger (and also much smaller) than the mean-free-path.
- For applications to the Earth's cloudy atmosphere, the observed optical variability, which indeed has long-range correlations shaped by small- and large-scale turbulence, leads to propagation kernels with power-law tails.

[23] An improved upper BC would capture the fact that some of the sunlight is transmitted quasi-ballistically through the top layer, but this would call for at least two new parameters (solar zenith angle and the partition between diffuse and collimated illumination).

I also critically re-examined the impact of sub-exponential free-path distributions on multiple scattering in finite media. Guided by early successes of a phenomenological model for solar photon propagation through the cloudy atmosphere based on Lévy (rather than Gaussian) random walks, I proposed here a new 1D transport model with propagation kernels having power-law tails as well as the proper near-field behavior. These kernels are particularly well adapted to problems of large-scale radiative transfer in the cloudy atmosphere since they follow directly from the observed Gamma-type distributions of optical variability. This new transport equation is solved numerically using a modified Monte Carlo scheme. The new model explains all the features of recent observations of the mean *and* RMS pathlengths of solar photons eventually transmitted to the ground in a narrow field-of-view around the zenith direction. In particular, we conclude that large-scale radiation transport in the cloudy atmosphere is in a pre-asymptotic regime where the thickness of the radiative boundary-layer (a couple of actual mean-free-paths) is commensurate with the outer thickness of the medium (from ground level to the top of the highest cloud).

In general, the new transport model based on effective propagation kernels offers a flexible intermediate approach to the perennial problem of unresolved variability. It is not as simple as homogenization, but it does avoid its main limitation. Nor is it as complicated as the coupled mean-field transport equations for random Markovian media, even in the two-state case. So one hopes to see applications in a wide variety of transport problems in both engineering and natural sciences.

Acknowledgments

Sustained financial support is acknowledged from the U.S. DOE's Atmospheric Radiation Measurement (ARM) Program over the long period during which this research was conducted. The author thanks Howard Barker, Brian Cairns, Hélène Frisch, Lee Harrison, Andrew Heidinger, Yong-Xiang Hu, Yuri Knyazikhin, Alexander Kostinski, Edward Larsen, Shaun Lovejoy, Alexander Marshak, Qi-Long Min, Jim Morel, Klaus Pfeilsticker, Sydney Redner, Graeme Stephens, and Warren Wiscombe for stimulating discussions around the topics of this paper both in person and in across the internet. Special thanks go to Igor Polonsky for the timely help in refining the numerics in Fig. 10 and much of the LaTeX source material. I wish to thank the volume editor, Frank Graziani, for his help, his patience, and the passion he put into bringing to life the series of interdisciplinary Computational Transport Workshops.

Finally, I dedicate this paper to the loving memory of my late father, John F. Davis, M.Eng., M.D., who passed away during the time of its writing. By boldly shifting careers multiple times, moving family-and-all to a new "old" country, and traveling far and wide beyond there, he gave meaning to the proverbial *path less-traveled*. More to the point of this paper, he demonstrated that the occasional large jump enables the traveler to sample more effectively the vast possibilities that inhabit geographical- and/or career-spaces, given the unknown but finite time of travel. I've tried to follow his example in taking those same kinds of steps/jumps both in real space and in "interest space" and, sure enough, many of my moves proved (so far) to be at once risky and wise. At least I've learned to look forward to the next destination and to welcome the next challenge.

References

1. D. Mihalas. *Stellar Atmospheres*. Freeman, San Francisco (CA), 2nd edition, 1979.
2. O.A. Avaste and G.M. Vainikko. Solar radiative transfer in broken clouds. *Izv. Acad. Sci. USSR Atmos. Oceanic Phys.*, 10:1054–1061, 1974.
3. G.C. Pomraning. *Linear Kinetic Theory and Particle Transport in Stochastic Mixtures*. World Scientific Publishing, Singapore, 1991.
4. G.L. Stephens. Radiative transfer through arbitrary shaped optical media, II: Group theory and simple closures. *J. Atmos. Sci.*, 45:1837–1848, 1988.
5. H.W. Barker. A parameterization for computing grid-averaged solar fluxes for inhomogeneous marine boundary layer clouds - Part 1, Methodology and homogeneous biases. *J. Atmos. Sci.*, 53:2289–2303, 1996.
6. H.W. Barker and A.B. Davis. Approximation methods in atmospheric 3D radiative transfer, Part 2: Unresolved variability and climate applications. In *3D Radiative Transfer in Cloudy Atmospheres*. A. Marshak and A.B. Davis (eds.). Springer-Verlag, Heidelberg, pages 343–383, 2005.
7. F. Graziani and D. Slone. Radiation transport in 3D heterogeneous materials: Direct numerical simulation. In *Proceedings of the American Nuclear Society Winter Meeting, New Orleans, LA*. ANS, LaGrange Park (IL), 2003.
8. R.F. Cahalan. Bounded cascade clouds: Albedo and effective thickness. *Nonlinear Proc. Geophys.*, 1:156–167, 1994.
9. B. Cairns, A.A. Lacis, and B.E. Carlson. Absorption within inhomogeneous clouds and its parameterization in general circulation models. *J. Atmos. Sci.*, 57:700–714, 2000.
10. P.M. Gabriel and K.F. Evans. Simple radiative transfer methods for calculating domain-averaged solar fluxes in inhomogeneous clouds. *J. Atmos. Sci.*, 53:858–877, 1996.
11. G.W. Petty. Area-average solar radiative transfer in three-dimensionally inhomogeneous clouds: The independently scattering cloudlets model. *J. Atmos. Sci.*, 59:2910–2929, 2002.
12. M.F. Shlesinger, G.M. Zaslavsky, and U. Frisch (eds.). *Lévy Flights and Related Topics in Physics*. Springer-Verlag, New York (NY), 1995.
13. G. Samorodnitsky and M.S. Taqqu. *Stable Non-Gaussian Random Processes*. Chapman and Hall, New York (NY), 1994.
14. K. Pfeilsticker. First geometrical pathlengths probability density function derivation of the skylight from spectroscopically highly resolving oxygen A-band observations. 2. Derivation of the Lévy-index for the skylight transmitted by mid-latitude clouds. *J. Geophys. Res.*, 104:4101–4116, 1999.
15. T. Scholl, K. Pfeilsticker, A.B. Davis, H. Klein Baltink, S. Crewell, U. Löhnert, C. Simmer, J. Meywerk, and M. Quante. Path length distributions for solar photons under cloudy skies: Comparison of measured first and second moments with predictions from classical and anomalous diffusion theories. *J. Geophys. Res.*, 2005 (in press).
16. A.B. Davis and Yu. Knyazikhin. A Primer in 3D Radiative Transfer. In *3D Radiative Transfer in Cloudy Atmospheres*. A. Marshak and A.B. Davis (eds.). Springer-Verlag, Heidelberg, pages 153–242, 2005.
17. D. Deirmendjian. *Electromagnetic Scattering on Spherical Polydispersions*. Elsevier, New York (NY), 1969.

18. Yu. Knyazikhin, A. Marshak, W.J. Wiscombe, J. Martonchik, and R.B. Myneni. A missing solution to the transport equation and its effect on estimation of cloud absorptive properties. *J. Atmos. Sci.*, 59:3572–3585, 2002.
19. M. Abramowitz and I.A. Stegun (eds.). *Handbook of Mathematical Functions with Formulas, Graphs, and Mathematical Tables*. US Govt. Printing Office, Washington (DC), 1964.
20. L.C. Henyey and J.L. Greenstein. Diffuse radiation in the galaxy. *Astrophys. J.*, 93:70–83, 1941.
21. A. Davis, S. Lovejoy, and D. Schertzer. Supercomputer simulation of radiative transfer in multifractal cloud models.In *IRS'92: Current Problems in Atmospheric Radiation*. S. Keevallik and O. Kärner (eds.). A. Deepak Publishing, Hampton (VA), pages 112–115, 1993.
22. A. Schuster. Radiation through a foggy atmosphere. *Astrophys. J.*, 21:1–22, 1905.
23. W.E. Meador and W.R. Weaver. Two-stream approximations to radiative transfer in planetary atmospheres: A unified description of existing methods and a new improvement. *J. Atmos. Sci.*, 37:630–643, 1980.
24. N.G. van Kampen. Stochastic differential equations. *Physics Reports (Phys. Lett. C)*, 24:171–228, 1976.
25. F. Reif. *Fundamentals of Statistical and Thermal Physics*. McGraw-Hill, New York (NY), 1965.
26. A.B. Kostinski. On the extinction of radiation by a homogeneous but spatially correlated random medium. *J. Opt. Soc. Amer. A*, 18:1929–1933, 2001.
27. A.B. Davis and A. Marshak. Photon propagation in heterogeneous optical media with spatial correlations: Enhanced mean-free-paths and wider-than-exponential free-path distributions. *J. Quant. Spectrosc. Radiat. Transfer*, 84:3–34, 2004.
28. W. Feller. *An Introduction to Probability Theory and its Applications*. Wiley, New York (NY), 1971.
29. U. Frisch and G. Parisi. A multifractal model of intermittency. In *Turbulence and Predictability in Geophysical Fluid Dynamics*, M. Ghil, R. Benzi, and G. Parisi (eds.), North Holland, Amsterdam (The Netherlands), pages 84–88, 1985.
30. A. Marshak, A. Davis, W.J. Wiscombe, and R.F. Cahalan. Scale-invariance of liquid water distributions in marine stratocumulus, Part 2 - Multifractal properties and intermittency issues. *J. Atmos. Sci.*, 54:1423–1444, 1997.
31. H.-O. Peitgen and D. Saupe. *The Science of Fractal Images*. Springer-Verlag, New York (NY), 1988.
32. R.F. Cahalan, W. Ridgway, W.J. Wiscombe, T.L. Bell, and J.B. Snider. The albedo of fractal stratocumulus clouds. *J. Atmos. Sci.*, 51:2434–2455, 1994.
33. H.W. Barker, J.-J. Morcrette, and G.D. Alexander. Broadband solar fluxes and heating rates for atmospheres with 3D broken clouds. *Quart. J. Roy. Meteor. Soc.*, 124:1245–1271, 1998.
34. J.W. Goodman. *Statistical Optics*. Wiley, New York (NY), 1985.
35. L.D. Landau and E.M. Lifshitz. *Statistical Physics*. Pergamon, New York (NY), 3rd edition, 1980.
36. L. Mandel and E. Wolf. *Optical Coherence and Quantum Optics*. Cambridge U. Press, New York (NY), 1995.
37. H.W. Barker, B.A. Wielicki, and L. Parker. A parameterization for computing grid-averaged solar fluxes for inhomogeneous marine boundary layer clouds - Part 2, Validation using satellite data. *J. Atmos. Sci.*, 53:2304–2316, 1996.

38. A. Marshak, A. Davis, W.J. Wiscombe, and R.F. Cahalan. Radiative smoothing in fractal clouds. *J. Geophys. Res.*, 100:26,247–26,261, 1995.
39. R.A. Shaw, A.B. Kostinski, and D.D. Lanterman. Super-exponential extinction of radiation in a negatively-correlated random medium. *J. Quant. Spectrosc. Radiat. Transfer*, 75:13–20, 2002.
40. A. Davis and A. Marshak. Lévy kinetics in slab geometry: Scaling of transmission probability. In *Fractal Frontiers*. M.M. Novak and T.G. Dewey (eds.). World Scientific, Singapore, pages 63–72, 1997.
41. A.G. Borovoi. On the extinction of radiation by a homogeneous but spatially correlated random medium: Comment. *J. Opt. Soc. Amer. A*, 19:2517–2520, 2002.
42. A.G Borovoi. Radiative transfer in inhomogeneous media. *Dokl. Akad. Nauk SSSR*, 276:1374–1378, 1984 (in Russian).
43. A.B. Kostinski. On the extinction of radiation by a homogeneous but spatially correlated random medium: Reply to comment. *J. Opt. Soc. Amer. A*, 19:2521–2525, 2002.
44. E.P. Zege, A.P. Ivanov, and I.L. Katsev. *Image Transfer Through a Scattering Medium*. Springer-Verlag, New York (NY), 1991.
45. K.M. Case and P.F. Zweifel. *Linear Transport Theory*. Addison-Wesley, Reading (MA), 1967.
46. E. Sparre Anderson. On the fluctuations of sums of random variables. *Math Scand.*, 1:236–285, 1953.
47. U. Frisch and H. Frisch. Universality in escape from half space of symmetrical random walks. In *Lévy Flights and Related Topics in Physics*, M.F. Shlesinger, G.M. Zaslavsky, and U. Frisch (eds.), Springer-Verlag, New York (NY), pages 262–268, 1995.
48. G.L. Stephens. Reply (to Harshvardhan and Randall). *Mon. Wea. Rev.*, 113:1834–1835, 1985.
49. G.L. Stephens, A.K. Heidinger, and P.M. Gabriel. Photon paths and cloud heterogeneity: An observational strategy to assess effects of 3D geometry on radiative transfer. In *3D Radiative Transfer in Cloudy Atmospheres*. A. Marshak and A.B. Davis (eds.). Springer-Verlag, Heidelberg, pages 587–616, 2005.
50. W.M. Irvine. The formation of absorption bands and the distribution of photon optical paths in a scattering atmosphere. *Bull. Astron. Inst. Neth.*, 17:226–279, 1964.
51. V.V. Ivanov and Sh. A. Sabashvili. Transfer of resonance radiation and photon random walks. *Astrophysics and Space Science*, 17:13–22, 1972.
52. K. Pfeilsticker, F. Erle, O. Funk, H. Veitel, and U. Platt. First geometrical pathlengths probability density function derivation of the skylight from spectroscopically highly resolving oxygen A-band observations: 1. Measurement technique, atmospheric observations, and model calculations. *J. Geophys. Res.*, 103:11,483–11,504, 1998.
53. Q.-L. Min and L.C. Harrison. Joint statistics of photon pathlength and cloud optical depth. *Geophys. Res. Lett.*, 26:1425–1428, 1999.
54. Q.-L. Min, L.C. Harrison, P. Kiedron, J. Berndt, and E. Joseph. A high-resolution oxygen A-band and water vapor band spectrometer. *J. Geophys. Res.*, 109:D02202, doi:10.1029/2003JD003540, 2004.
55. Q.-L. Min, L.C. Harrison, and E.E. Clothiaux. Joint statistics of photon pathlength and cloud optical depth: Case studies. *J. Geophys. Res.*, 106:7375–7385, 2001.

56. R.W. Portmann, S. Solomon, R.W. Sanders, J.S. Daniel, and E. Dutton. Cloud modulation of zenith sky oxygen path lengths over Boulder, Colorado: Measurement versus model. *J. Geophys. Res.*, 106:1139–1155, 2001.
57. M. Quante, H. Lemke, H. Flentje, P. Francis, and J. Pelon. Boundaries an internal structure of mixed phased clouds as deduced from ground-based 95-Ghz radar and airborne lidar measurements. *Phys. Chem. Earth*, 25:889–895, 2000.
58. A.B. Davis and A. Marshak. Space-time characteristics of light transmitted through dense clouds: A Green function analysis. *J. Atmos. Sci.*, 59:2714–2728, 2002.
59. W.J. Wiscombe and G.W. Grams. The backscattered fraction in two-stream approximations. *J. Atmos. Sci.*, 33:2440–2451, 1976.
60. J. Lenoble (ed.). *Radiative Transfer in Scattering and Absorbing Atmospheres: Standard Computational Procedures*. A. Deepak Publishing, Hampton (VA), 1985.
61. S.V. Buldyrev, M. Gitterman, S. Havlin, A.Ya. Kazakov, M.G.E. da Luz, E.P. Raposo, H.E. Stanley, and G.M. Viswanathan. Properties of Lévy flights on an interval with absorbing boundaries. *Physica A*, 302:148–161, 2001.
62. G. Marchuk, G. Mikhailov, M. Nazaraliev, R. Darbinjan, B. Kargin, and B. Elepov. *The Monte Carlo Methods in Atmospheric Optics*. Springer-Verlag, New York (NY), 1980.
63. H.C. van de Hulst. *Multiple Light Scattering: Tables, Formulae and Applications*. Academic Press, San Diego (CA), 1980.